Analysis of 3D-Printed Fin Performance

by

Cassandra M. Wright

A thesis submitted in partial fulfillment of

the requirement for the degree of:

Master of Science

(Mechanical Engineering)

at the

UNIVERSITY OF WISCONSIN-MADISON

2018

Approved by:

_____ Date: _____

Professor Gregory F. Nellis

Table of Contents

List of Figures

1. Introduction

1.1. ARID program

The Advanced Research in Dry-Cooling program (ARID) is funded through the Department of Energy's Advanced Research Projects Agency-Energy division. The main goal of this initiative is to reduce water consumption associated with power production. Most power plants today use heat rejection systems that consume water, often in the form of cooling towers. Therefore, one objective of this program is to research more efficient dry-cooled heat exchangers that can ultimately be used in a power plant with limited access to water. Figure 1 shows the predicted water consumption for thermo-electric power generation by the year 2035:

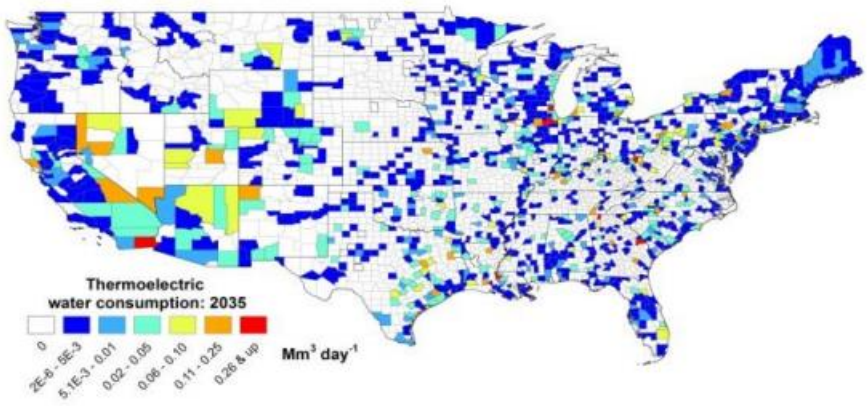

Figure 1: Predicted U.S. water consumption due to thermoelectric power generation in 2035 [2]

The West and Southwest were identified as regions with limited water availability, meaning regions where the water demand is more than 70% of the water supply [2]. These regions

would benefit most from advancements in air-cooling technology. Using air at room temperature to cool the working fluid of a cycle requires a higher efficiency to maintain the same level of cooling that is achieved using water. Over 60% of the energy produced from thermoelectric powerplants is waste-heat [1]. In order to remove this heat from the system, most power plants use wet-cooling systems. It is estimated that more than 40% of withdrawals from fresh water sources can be attributed to wet-cooling in power plants, corresponding to 139 billion gallons of water per day [1]. In an effort to conserve water resources, the ARID program aims to advance dry-cooling technology to be competitive with current wet-cooling technology. Not only would dry-cooling in power plants conserve fresh water supplies, but it would expand the range of possible future locations of power plants to geographic areas without large bodies of fresh water nearby. In order to optimize dry-cooling, the geometry on the airside portion of the heat exchanger must be optimally designed.

1.2. Additive Manufacturing

Additive manufacturing, or 3D-printing, was selected as the manufacturing process to create the heat exchanger to be used for dry-cooling. Additive manufacturing allows the freedom to explore unique fin and channel designs that would be too complicated and costly for traditional manufacturing methods. Fused Filament Fabrication (FFF) is an additive manufacturing process that deposits a continuous stream of thermoplastic from the nozzle as it moves across the build plane. This manufacturing method has been available since the 1980s, so it is well understood. While heat exchangers are typically made from copper,

aluminum, or other conductive materials, the base material for FFF is a polymer. The polymer filament can be infused with metals to increase conductivity, as well as antimicrobials to decrease heat exchanger downtime due to cleaning and other maintenance. Because additive manufacturing is a relatively new technology in the heat exchanger industry, little research has been done on how the manufacturing process affects the performance.

2. Heat Exchanger Geometry

2.1. Heat Exchanger Layout

The ultimate goal of this research is to design a heat exchanger that can be implemented in a dry cooled power plant. This work revolves around the design of a small-scale heat exchanger module; several such modules would be required to provide a full-scale dry cooled heat exchanger suitable for a power plant. The size of the heat exchanger studied here could also be used directly in a typical air handler in an HVAC system.

The demonstrator model of the heat exchanger has a 12-inch by 12-inch frontal area and allows for approximately 1 to 2 inches in the direction of flow on the air-side. The general layout of the heat exchanger can be seen in Figure 2.

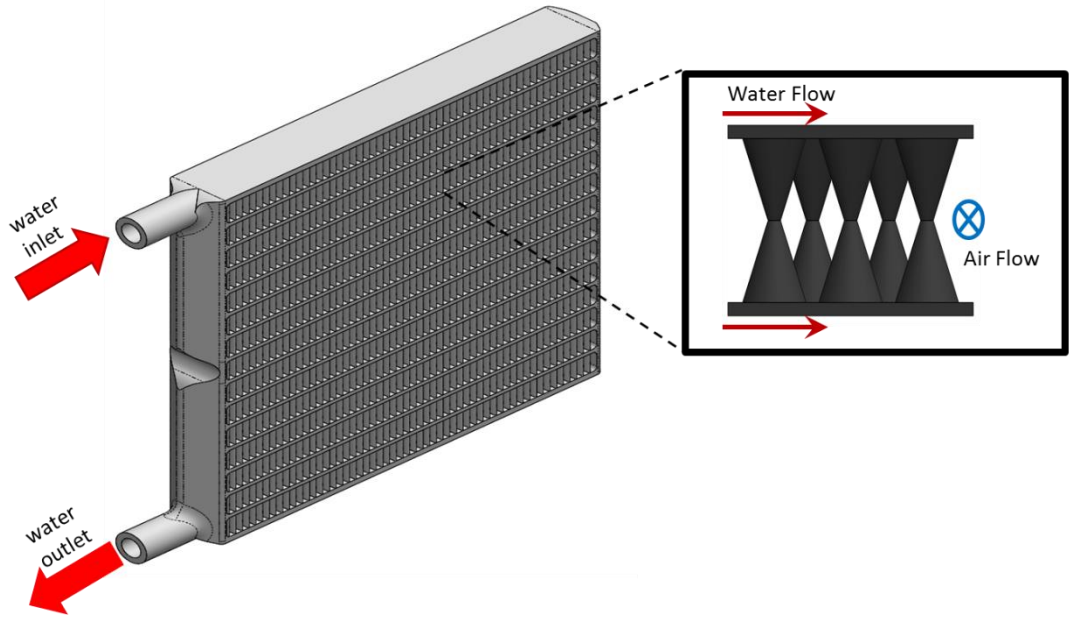

Figure 2: Heat exchanger design

The small length of flow on the airside is related to the requirements on pressure drop that stem from the use of fans to pull air across the core. The fin geometry must be optimized to provide the necessary amount of heat transfer given this envelope which generally leads to fin dimensions that are on the scale of millimeters.

2.2. Correlation Implementation and Experimental Results

A tapered pin was selected as an initial fin geometry for further analysis. In order to optimize the performance of the heat exchanger, correlations for the tapered fin geometry were created using dimensionless parameters [3]. The tapered fin correlations provided the Nusselt number (dimensionless heat transfer coefficient) as a function of the following parameters:

- Reynolds number

- longitudinal and transverse pitches, S_T and S_L
- fin height, h
- degree of taper of the fin, T

The geometric parameters incorporated in the formulation of the correlations are shown in Figure 3.

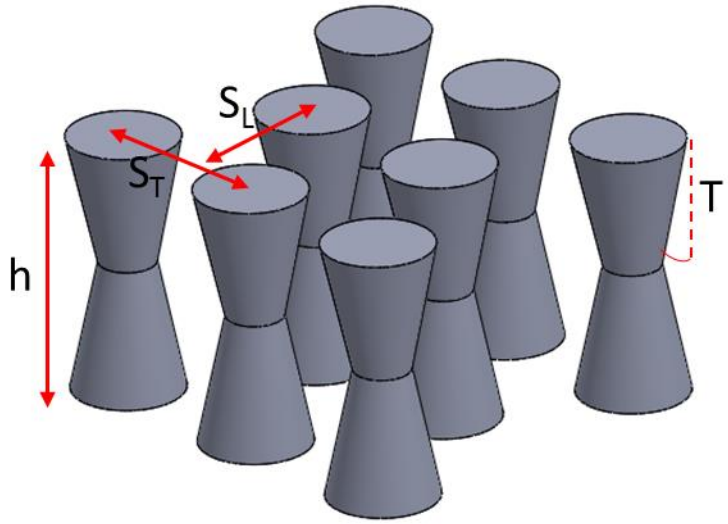

Figure 3: Geometric parameters of tapered pin fins

Hundreds of CFD simulations were run for individual geometries, that assumed a smooth fin surface, in order to obtain information over a range of each of the dimensionless parameters listed above. Correlations were developed from these results to predict the performance of a given fin geometry. The correlations were implemented in an overall heat exchanger model and used to design several modules that were then fabricated and tested [4]. The experimental data and the model performance can be found in Figure 4.

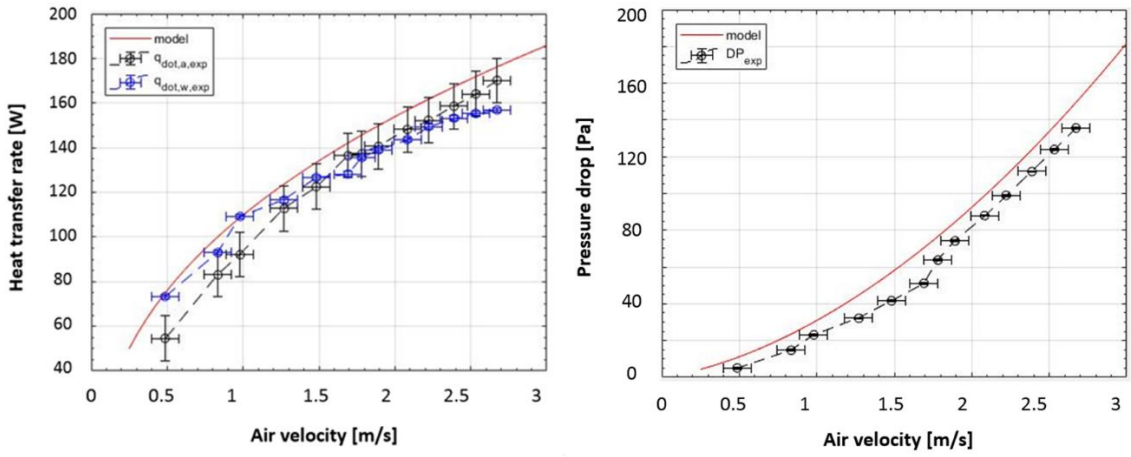

Figure 4: Thermal and hydraulic model performance compared to experimental results [4]

The results shown in the figures above are typical of other data collected for fins over a wide range of geometric parameters. Data was collected for both the air-side and water-side streams in order validate the experiment. In general, agreement between the model results generated from smooth surface correlations agreed well (within approximately 10%) of the measured performance even though the actual geometry was not smooth, as discussed in the subsequent section.

2.3. 3D-Printing Fins

Upon inspection of the printed fins it was clear that they were not printed with a smooth surface. It is therefore surprising that there is such good agreement between the model, which implements correlations based on smooth surfaces, and experimental data collected from heat exchangers that were 3D-printed. The heat exchangers are printed layer by layer which means that the fins themselves are printed a single layer at a time. For a fin with a

build direction oriented as shown in Figure 5, the printing process would look something like Figure 6.

Figure 5: Tapered pin fin

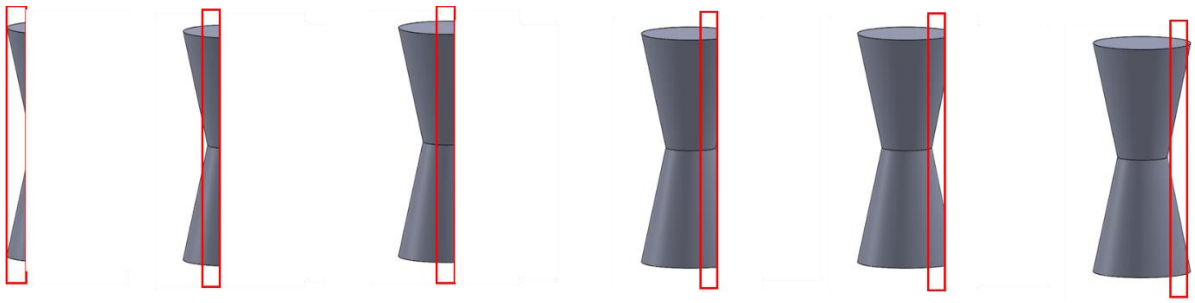

Figure 6: Example layers of 3D-printed tapered pin fin

The first layers of the fin have minimal support structure as they each protrude from the lower layers by some amount. As the taper becomes less severe, the material from the first half of the fin can be forced, by gravity, to sag. Once the first half (i.e., bottom) of the fin is printed, the remaining layers have a complete surface on which they are built. An added benefit of the tapered geometry is that the tool-pathing of the nozzle is continuous. The nozzle deposits material for the top half of the fin, followed by the bottom half. In this

manner, the nozzle does not have to stop depositing material at any point in the middle of the fin. Figure 7 shows the path a nozzle might take for various layers of a fin.

Figure 7: Tool-pathing for various layers of tapered fin

Figure 8 is a 3D-rendering of CT scans taken of a single tapered fin within a heat exchanger. There is a 90-degree rotation between each view of the fin rendering. Figure 8.A shows the layers that were first printed (i.e., the bottom). There is considerable sagging in this material. The print direction in this rendering is into the page. Figure 8.B displays how the fin was built with individual layers. The build direction in this rendering is from left to right. Figure 8.C displays the layers of the fin that printed after the first half of the fin was completed (i.e., the top of the fin). These layers were printed onto a surface, so there is no

sagging. The tool-pathing can very clearly be seen. The build direction for this view is out of the page.

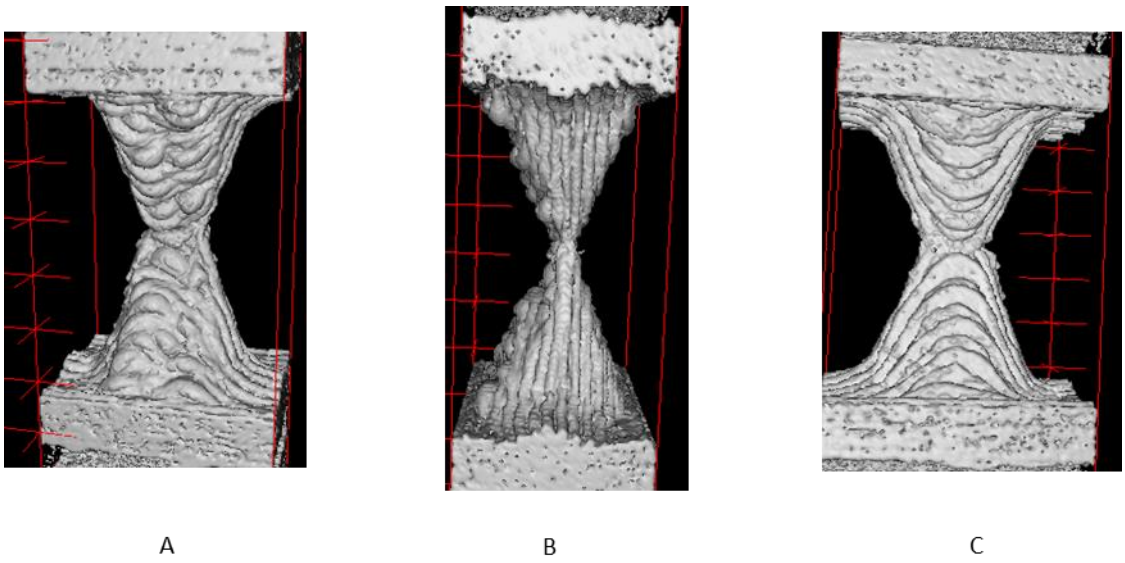

Figure 8: Rendering of CT scans of a single tapered fin

Multiple aspects of the manufacturing process such as print speed, extrusion ratio, build direction, bed temperature, and tool-pathing can impact print quality. Even with the correct combination of print properties, printing with polymers using fused filament fabrication cannot produce smooth, as-modeled surfaces. Figure 9 shows the cross-sections at various locations along the height of the tapered fins. The airflow over these fins is from the bottom of the page to the top.

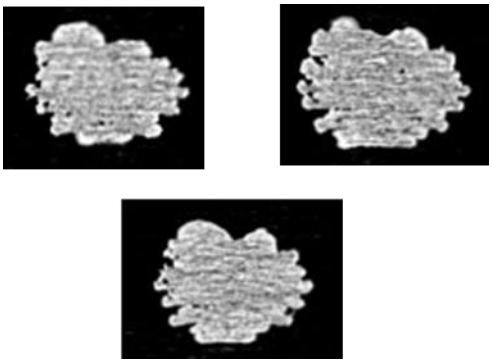

Figure 9: Cross-sections of tapered pin fin

The printed fins are generally circular in nature but have numerous bumps along the circumference. The larger bumps at the top of the fins pictured in Figure 9 correspond to the layers that printed first. The bumps on the fins are not merely surface roughness in the usual sense. These bumps are significant in size compared to the overall size of the fin. The correlations that were developed to predict the performance of tapered fins that are smooth and circular in cross-section, but experimentally we have found that they can accurately predict the performance of fins with bumpy surfaces. Understanding why the smooth surface correlations can accurately predict the performance of bumpy fins and the general effect of the "bumpiness" is the motivation for this work.

3. Opposed Waviness Geometry

3.1. Geometry

In order to characterize the waviness associated with the printed fins, a series of simulations was performed to understand the effect that bumps have on fin performance. For the fins shown in the CT scans in the previous section, the bumps that were created

around the edge of the fins *oppose* the flow; that is, the flow direction is perpendicular to the direction of each bead that makes up the fin. To create a simulation that mimics the situation created with the printed fins, a sine wave circumscribed onto a circular fin was created. Below, in Figure 10.A, is the basic geometry of the fin. For all simulations, the sine wave is centered on the circumference line, so the average diameter remains constant at 6 mm.

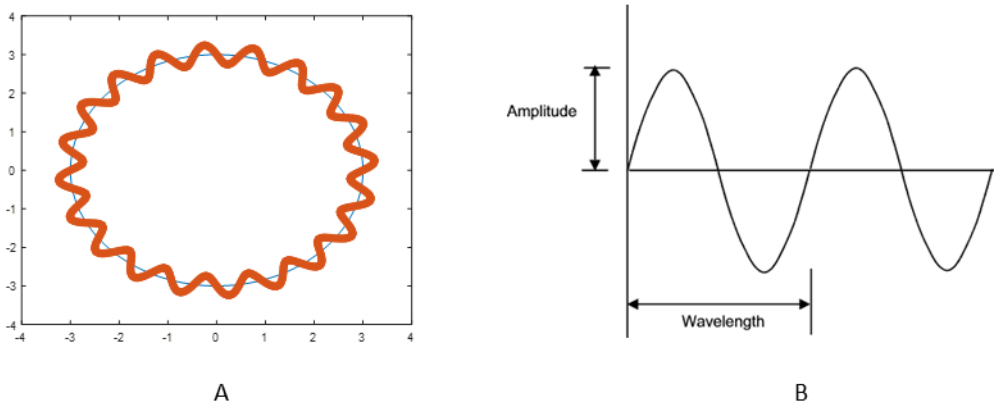

Figure 10: Sinewave circumscribed on a circle

For the majority of the as-printed fins, the ratio of the height of the bumps on the fin to the overall diameter is less than 0.05 and the ratio of the wavelength length of the bump to the overall diameter is less than 0.1. The bumps vary widely in size on a single fin, as well as from fin to fin. However, these ratios guided the ranges used in the parametric study. The amplitude of a sinewave refers to the height of the wave. The wavelength refers to the distance it takes to create a complete sinewave. These characteristics of a sinewave are detailed in Figure 10.B. For a longer wavelength, there will be less sinewaves over the same distance. Below are the 4 wavelengths that were simulated, at a given amplitude. The

number of sinewaves, or frequency, varies from 10 to 40, corresponding to wavelengths from 1.88 mm to 0.47 mm, respectively. Figure 11 shows what the variation in wavelength physically looks like for a given amplitude.

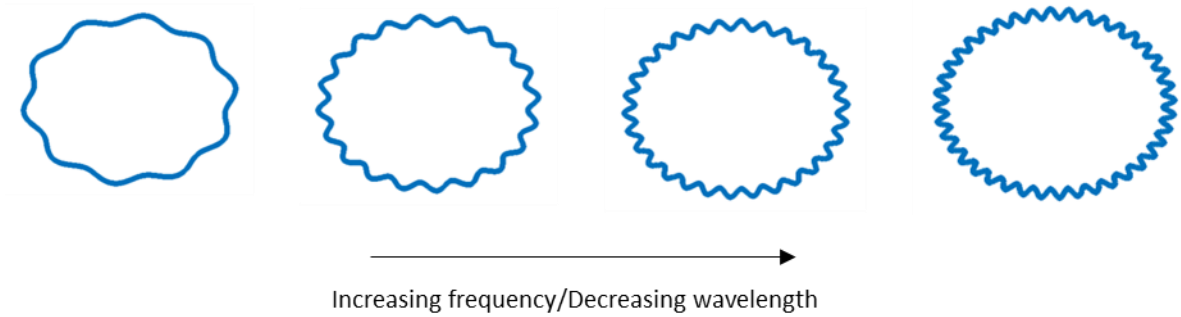

Figure 11: Fins with varying frequencies/wavelengths

For comparison purposes, the parameters of interest are the dimensionless ratios of amplitude to diameter and wavelength to diameter.

The simulations were performed using ANSYS Fluent. The geometry was created using a MATLAB code that generated 1500 points, taking the frequency, which corresponds to wavelength, and amplitude as inputs. The points were then exported to a text file, according to the format specified by ANSYS. A portion of this text file can be found in Figure 12.

```
#Group  Point   X       Y       Z
1       1       3.000   0.000   0
1       2       3.013   0.008   0
1       3       3.025   0.015   0
1       4       3.037   0.023   0
1       5       3.050   0.031   0
1       6       3.062   0.038   0
```

Figure 12: Coordinate text file imported into DesignModeler

This code can be found in Appendix A. A coordinates file was created and imported directly into DesignModeler, which generated points in a single plane. A spline curve was used to connect the points and create the 2-dimensional fin. Because the geometry of the fin only varies in two dimensions, a 2-dimensional simulation was appropriate and more computationally efficient. The simulation was performed in two dimensions to mimic an infinitely long fin. A 3-dimensional view of the fin can be found below in Figure 13. In this view, the airflow is into the page.

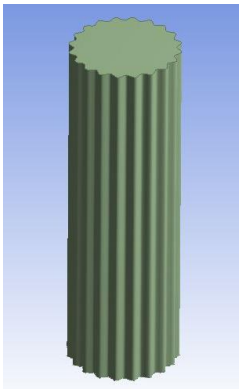

Figure 13: 3-Dimensional opposed waviness fin

3.2. Set-up

The fluid domain around the fin was restricted to represent a single fin in a bank of closely spaced fins. The spacing between the fins was held constant, while the amplitude and frequency of the bumps was modified. The average diameter of the fin was held constant, at 6 mm, and the fluid domain box was held at 8-mm by 8-mm. Figure 14 shows an array of fins with the fluid domain used in the simulation. Note that as the amplitude of the bumps increased, the minimum flow area between adjacent fins decreased.

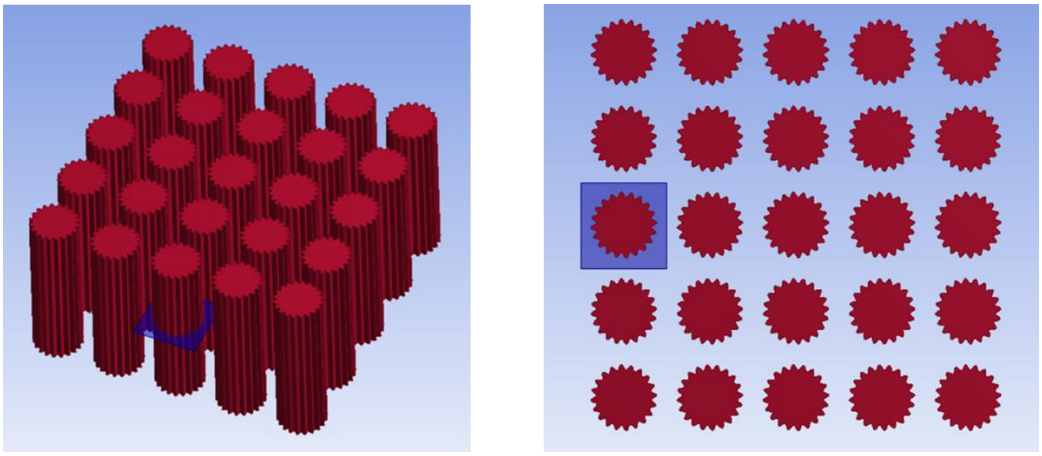

Figure 14: Array of wavy fins

The boundary conditions for the simulation are detailed in Figure 15. The fluid flow for the simulations is from the bottom of the page to the top of the page. The boundary at the inlet of the fluid domain was a velocity inlet. An air velocity was specified, along with a fluid inlet temperature, T_{in}, of 300 K. The range for air velocities was 0.6 m/s to 5 m/s, corresponding to Reynolds numbers from 225 to 1800. The Reynolds number range was guided by the range over which the heat exchangers are tested. The boundary at the outlet was set to a pressure outlet, with 0 Pa Gauge pressure and a backflow temperature of 300 K. The symmetry boundary conditions were applied to either side of the fluid domain cell, to mimic the effect of multiple fins. The fin temperature, T_s, was held at a constant 400 K.

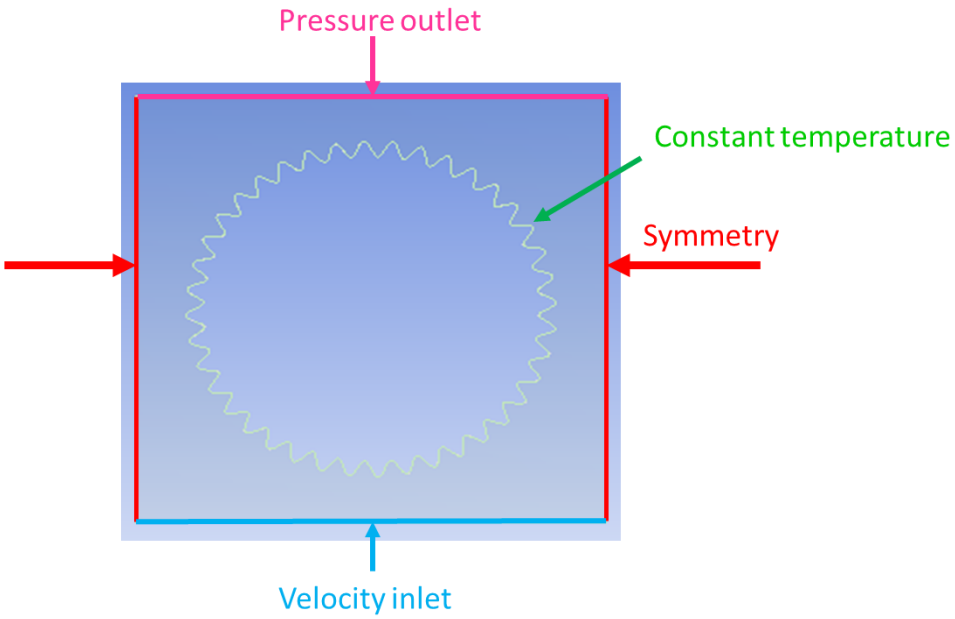

Figure 15: Boundary conditions for ANSYS model

The fluid properties for the air were kept constant. The temperature of the air for all simulations varied by less than 40 K, so the change in the fluid properties over the temperature range was negligible and allowed for easier computation. The air properties specified in Fluent are detailed below in Table 1. These properties are taken from [5] for air at a temperature of 300 K.

Table 1: Air properties specified in Fluent

Fluid Property	
Density	1.1614 kg/m^3
Specific heat	1007 J/kg-K
Conductivity	26.3x10^{-3} W/m-K
Dynamic viscosity	184.6x10^{-7} N-s/m^2

A coupled solving scheme was used in Fluent to solve pressure and momentum simultaneously. A Green-Gauss Node based solution, which is highly accurate, was used to calculate the diffusion terms and velocities. A second order solver was used for more accuracy to solve the pressure. A third-order MUSCL (Monotonic Upwind Scheme for Conservation Laws) solver was used for momentum and energy which is useful for unstructured meshes and can more accurately predict secondary flows and vortices. The residuals for continuity and velocity in the x and y directions were specified to 1x10^{-4}. The residual for energy was specified to 1x10^{-6}. An iteration limit of 1000 was also specified. The iteration limit allows for the simulation to end if the convergence has not been reached.

3.3. Mesh

The complex curvature associated with the surface when simulating large amplitudes and frequencies required the triangle meshing method that is typically used for curved edges. This method was applied to the entire fluid domain. The spline that was formed by the coordinate file was a non-uniform rational b-spline (NURBS) curve. The NURBS curve

requires a highly refined mesh in order to solve. The spline was refined based on the amplitude of the sinewave. The minimum number of elements suggested along any edge is 10. The refinement was specified to create at least 50 elements along the curve from the average radius, or start of the sinewave, to the peak/trough of the sinewave, or farthest point from the average radius. Complex flows are more easily captured with a refined mesh, which grows slowly. A growth rate of 1.05 was specified to create the mesh from the curve to the outer edge of the fluid domain. A smaller growth rate was necessary for model convergence and an accurate energy solution, which required a larger number of elements in the mesh throughout the fluid domain.

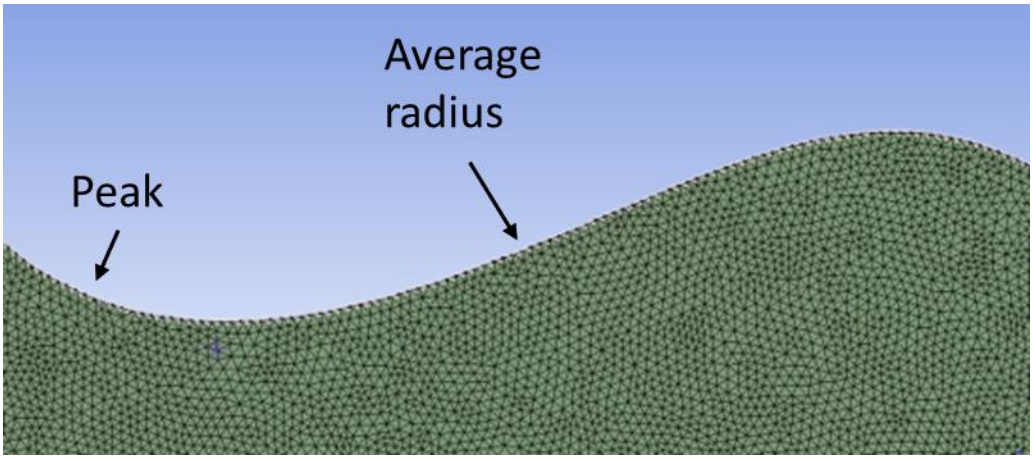

Figure 16: Refined mesh for opposed waviness fin

The refined mesh for a frequency of 10 and amplitude of 0.25 can be seen in Figure 16. The location of the trough and average radius are identified for reference.

3.4. Model Validation (Cylinder in Crossflow comparison)

The model was validated by comparison with correlations for a cylinder in crossflow. The purpose of these studies is to model the effect waviness has on a fin in a bank of fins. Therefore, the fluid domain was originally restricted to accomplish this. However, the correlation is for a cylinder in an infinite medium and therefore the fluid domain surrounding the fin was significantly increased in order to validate the model. The performance of a cylinder in crossflow with a restricted fluid domain could not be compared to established correlations because it would create more heat transfer and a larger pressure drop, due to the restricted area of flow. The amplitude of the sinewave was set to zero in order to create a circular fin. The geometry was created in the same way as the wavy fins with the same simulation set-up. Heat transfer coefficients were calculated over a range of inlet fluid velocities. A corresponding Nusselt number and Reynolds number were calculated. The fin performance was compared to established correlations found in [5]. The correlation is dependent on the Reynolds number and Prandtl number and is given by:

$$\overline{Nu} = \frac{\overline{h}D}{k} = C\, Re^{m}\, Pr^{1/3} \tag{1}$$

where:

$$C = 0.683 \text{ and } m = 0.466$$

for Reynolds numbers within the range of 40-4000. The Fluent results and correlations are compared in Figure 17.

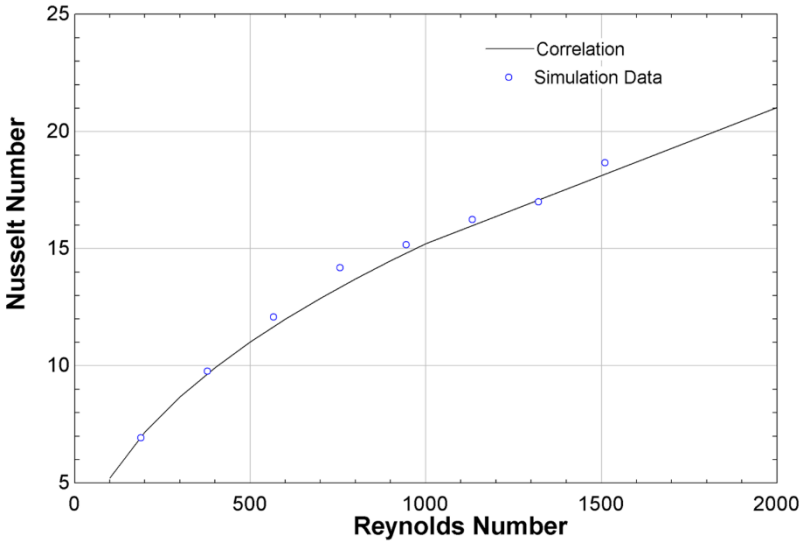

Figure 17: Cylinder in crossflow simulation and correlation results

The simulation results were all within 7% of the correlation predictions, validating the model used for the wavy fins.

3.5. Fin performance metrics

The correlations associated with the tapered fin predict the friction factor and the average Nusselt number, which describe the hydraulic and thermal performance, respectively. A corresponding pressure drop and heat transfer coefficient for a given geometry can then be calculated and implemented in the heat exchanger model. In order to compare the performance of a fin with a wavy surface to a smooth fin, the average heat transfer coefficient of the wavy fin, $\overline{h_{wavy}}$, was calculated and compared, in the form of a ratio, to the heat transfer coefficient of a smooth fin, $\overline{h_{smooth}}$. The method for calculating the heat transfer coefficient is detailed below. The mass flow rate, $\dot{m}$, the mass-weighted outlet temperature, T_{out}, and the inlet pressure, P_{in}, were all recorded outputs from every

simulation. Other inputs that were specified in the set-up were also used in the performance metrics. The effectiveness of the fin when considered to be a heat exchange surface was calculated and is given by the equation:

$$\varepsilon = \frac{T_{out} - T_{in}}{T_s - T_{in}} \tag{2}$$

which allowed for the calculation of the Number of Transfer Units (NTU) given by the equation:

$$NTU = -ln(1 - \varepsilon) \tag{3}$$

and finally, the conductance, UA, was calculated:

$$UA = \dot{m}c_p NTU \tag{4}$$

The average heat transfer coefficient of the fin can be calculated from the conductance, where S is the length of the curve and L is the arbitrary length into the page chosen as 1 m by Fluent for a 2-dimensional analysis:

$$\bar{h} = \frac{UA}{SL} \tag{5}$$

S is calculated using the formula for curve length defined for any set of parametric equations x and y with respect to θ:

$$S = \int_a^b \sqrt{\left(\frac{dx}{d\theta}\right)^2 + \left(\frac{dy}{d\theta}\right)^2}\, d\theta \tag{6}$$

The opposed waviness simulation is a 2-dimensional simulation, so the actual heat transfer coefficient can be found by multiplying the heat transfer coefficient per unit length by the length of the fin.

The pressure drop across the wavy fin was also calculated and then compared to the pressure drop across a smooth fin. The method for calculating the pressure drop is detailed below:

$$\Delta P = P_{in} - P_{out} \quad (7)$$

4. Aligned Waviness Geometry

4.1. Geometry

The opposed waviness simulation examined a flow that directly opposed the surface waves. Another simulation was designed to explore how the effect of surface waves that are *aligned* with the flow. In order to characterize the effects associated with the aligned waviness on a fin, a series of simulations was performed within the same geometric ranges seen in the opposed waviness study, which were selected based on observed geometries created by additive manufacturing. The surface area for a specific combination of amplitude and wavelength is equal for the opposed and aligned waviness studies. A given amplitude and frequency add the same amount of surface area to a fin for both the opposed and aligned studies. Figure 18 is a graphical representation of the geometric ratios that were explored in both studies. The area ratio is the exposed surface area of the wavy fin

compared to the surface area of a smooth fin with a diameter the same size as the average diameter of all wavy fins.

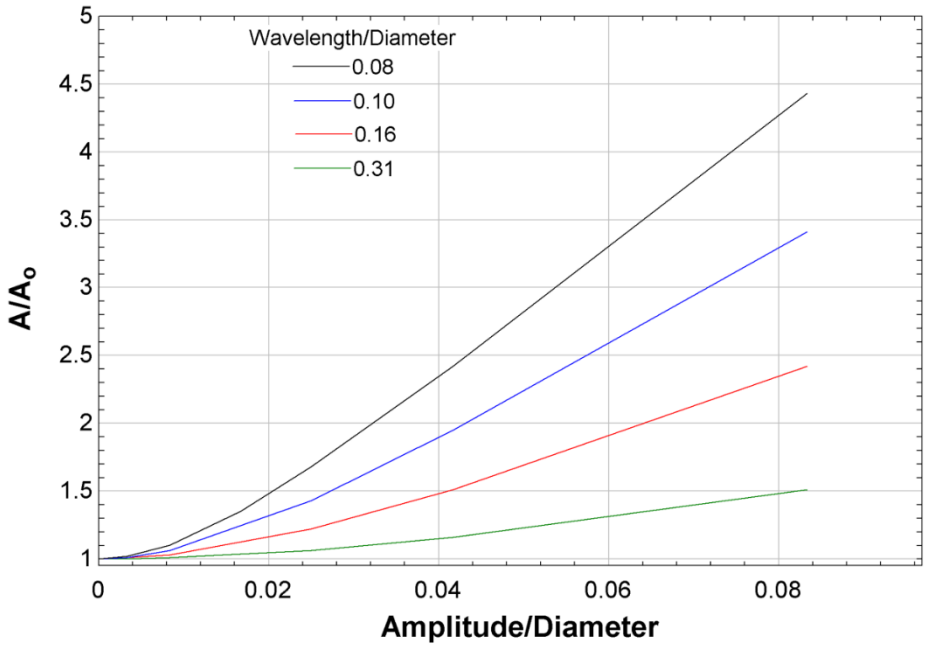

Figure 18: Area ratios for various geometric ratios

The aligned waviness creates a flow path that allows the air to go directly through (along) the wave as it flows over the fin surface. The geometry was created in a similar way as the opposed waviness fins. The code used to create the opposed waviness fins was slightly modified to create a sinewave along a vertical line, instead of one that is circumscribed on a circle. The code wrote data to a text file to create points that could be imported into DesignModeler. A cross-section created by the coordinate file can be found in Figure 19.A. The amplitude and wavelengths were varied, while the average diameter remained constant.

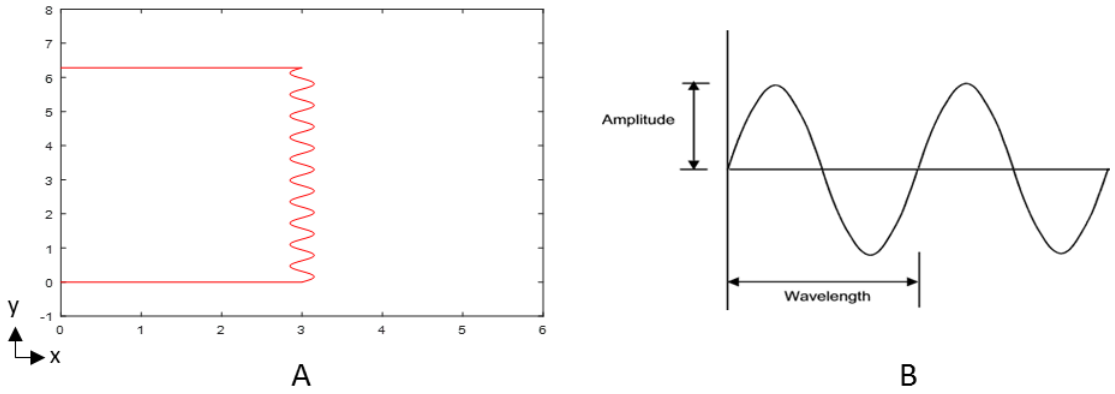

Figure 19: Sinewave along fin edge

The surface created represents the cross-section from the center of the fin to the outer edge of the fin. This surface was rotated about the y-axis to create the 3-dimensional fin, which is shown in Figure 20. The distance of the point farthest from the center of the fin increases with amplitude. The number of peaks located on the edge of the fin increases with a decreasing wavelength.

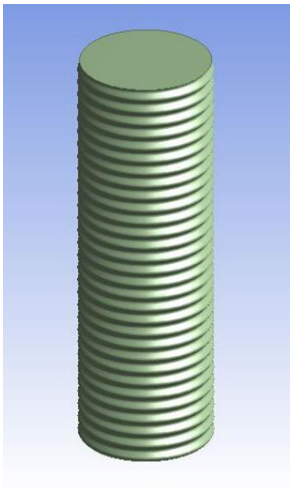

Figure 20: 3-dimensional aligned waviness fin

The airflow approaching the fin is into the page. The air can go directly through the sinewave as if travels over the fin. The fin geometry varies in all 3 dimensions, so a 3-dimensional simulation was necessary. A 3-dimensional simulation can capture the heat transfer at each location along the height of the fin, corresponding to a moving along the sinewave, and the heat transfer around the circumference of the fin.

4.2. Set-up

The fluid properties and solver settings from the opposed waviness simulation were applied to the aligned waviness simulation. The fluid domain was again restricted to mimic a single fin in an array of fins. The fluid domain was 3-dimensional, and the height of the fluid domain remained constant for all wavelengths. Figure 21 shows the symmetric boundaries that were applied in order to decrease the fluid domain. The number of bumps varied in the fluid domain, with varying wavelength. Geometric symmetry boundaries can be applied in order to decrease the size of the computational domain for ease of computation. A smaller domain was created by applying geometric symmetry boundaries to the top and bottom of the fluid domain.

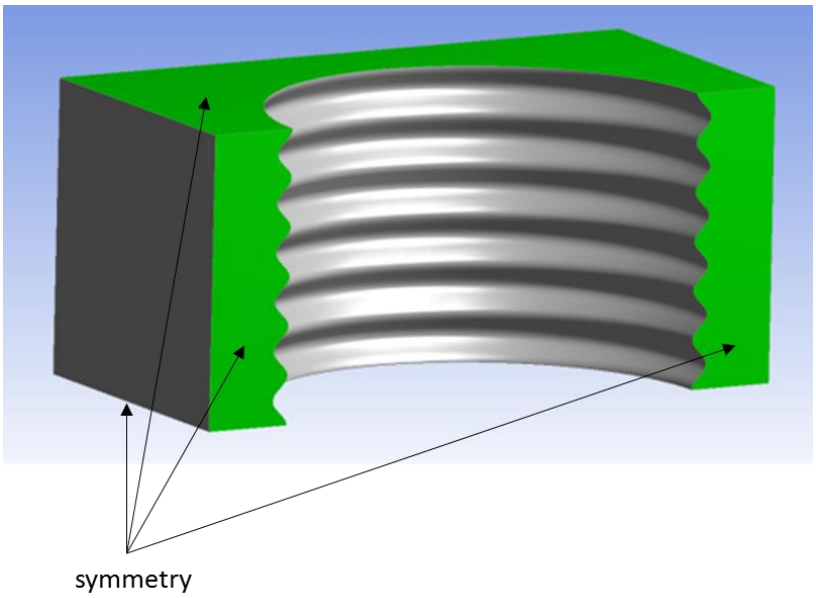

Figure 21: Symmetry boundaries for aligned waviness fin

In order to maintain the number of elements required (to a manageable level), a geometric symmetry boundary was also implemented through the middle of the fin. This boundary still allows for velocity-inlet and pressure-outlet conditions to be specified. The boundary conditions are identified below, in Figure 22.

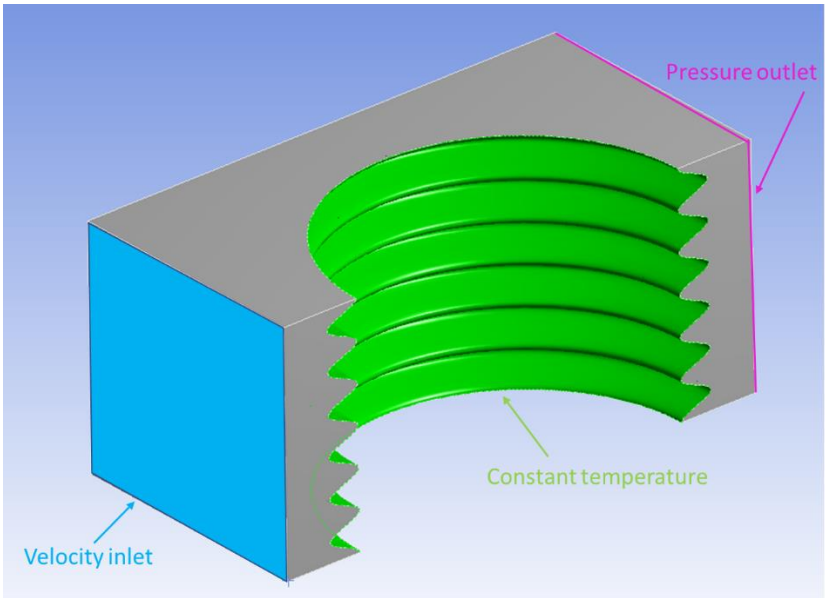

Figure 22: Boundary conditions for aligned waviness fin

The velocity-inlet was specified with an initial air velocity. The velocity and Reynolds number ranges from the opposed waviness simulations were used to allow for comparison between geometries. The flow for each simulation will start at the velocity-inlet and move around the circumference to the pressure-outlet.

4.3. Mesh

The tetrahedron method was applied to the entire fluid domain. The tetrahedrons are better for large curvature and more accurate when using inflation, because the elements tend to be more proportionate in all directions, including in the direction of flow. The geometric symmetry boundary on the top and bottom portion of the fluid domain also created areas that needed additional inflation. With increasing amplitudes and decreasing wavelengths, the portions of fluid at the top and bottom of the fluid domain become smaller. The smaller features require more elements to capture the true physics of the

model. The model was meshed with inflation on the face of the fluid that is exposed to the fin. An example mesh is shown in Figure 23.

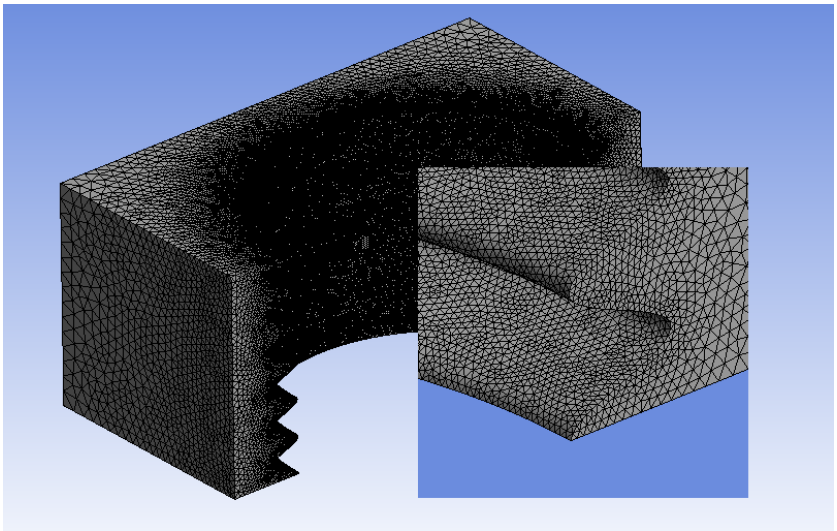

Figure 23: Aligned waviness mesh

Face sizing was the form of inflation used on the face of the fluid domain that was exposed to the fin. Face sizing requires that a minimum tetrahedron face size and edge length is specified, along with a maximum face size. The sizing was chosen based on the size of bump created by each combination of amplitude and wavelength. The growth rate of elements from the inner surface of the fluid domain to the outer surface also varied based on the face sizing. At the outer edge, a minimum of 10 elements was required. The mesh sensitivity was explored to ensure accurate results with a coarser mesh. This was performed using the geometry with the largest amplitude and shortest wavelength, which captured the geometric extremes. The study increased inflation on the face of the fin, as well as throughout the entire fluid domain. The finest mesh contained twice as many elements as the meshing method used for the entire aligned waviness study. There was only a 1%

difference in the standard mesh and the refined mesh with twice as many elements. This simulation required 3-dimensional elements as compared to the 2-dimensional elements from the opposed waviness study, so the aligned waviness study was inherently more computationally intense.

4.4. Fin performance metrics

The performance metrics to evaluate the fins were evaluated in the same way as the opposed waviness fins. Equation 5 describes the thermal performance metric of each fin, and Equation 6 describes the hydraulic performance of each fin.

5. Simulation Results

5.1. Opposed Waviness Results

5.1.1. Opposed waviness performance compared to smooth fin

A smooth fin in a restricted fluid domain behaves very similarly to a single cylinder in crossflow. Figure 24 shows the smooth fin results. The airflow in this figure is from bottom to top and the fin is infinitely long out of the page.

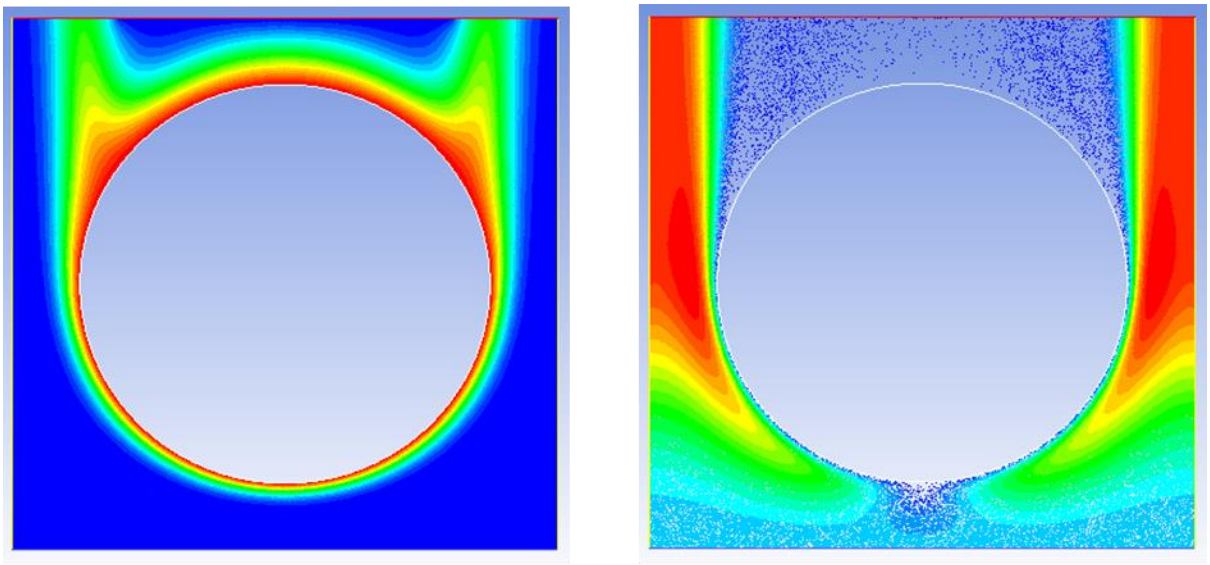

Figure 24: Smooth fin contours of (A) temperature and (B)velocity

Figure 24.A is a temperature contour plot where the warm air is red and the cool air is blue. The fin warms the air around it as is passes by. The temperature gradient in the air can be seen clearly surrounding the fin. The band of warm air around the circumference of the fin increases in thickness from the initial point of contact near the velocity-inlet to the pressure-outlet. Figure 24.B is the velocity vector plot for the smooth fin. The faster velocity air is red while the slower moving air is blue. The blue vectors indicate where the air first impinges on the fin. The air became almost stagnant at the stagnation point. The air accelerates around the sides of the fin where the air is warmed.

Figure 25 shows the same results (temperature and velocity) for the opposed wavelength simulation with a specific wavelength and amplitude combination. The airflow is again from the bottom of the page to the top of the page.

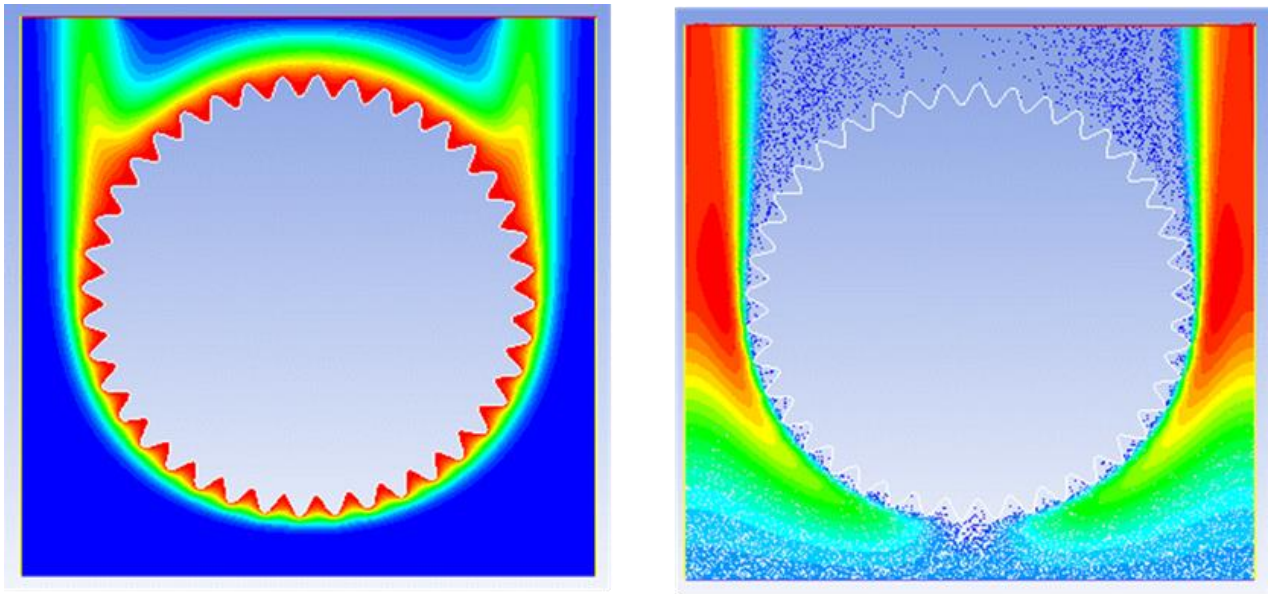

Figure 25: Opposed waviness contours of (A) temperature and (B) velocity

The results in Figure 25 resemble the results found in Figure 24 for the smooth fin. Figure 25.A shows a similar temperature profile as was observed for the smooth fin; however, in the troughs of the waves air is warmed to the wall temperature. There is another similar ring of heated air surrounding the fin. Where the flow initially comes in contact with the fin, the air at the average radius is not completely warmed to the fin temperature as it was in the smooth fin. The average radius is located in between the peak and trough of the sinewave. Figure 25.B contains a similar vector plot to that of the smooth fin. The location of initial air contact with the fin is stagnant, but there are other locations of nearly stagnant air in the wavy fin. The air within each trough is very slow-moving, almost stagnant. Because the velocity within the troughs is very low, the distance that conduction has to occur increases with amplitude. The temperature bands are not as warm, at various

circumferential locations, as the bands surrounding the smooth fin. The thermal boundary layer becomes thicker and the conduction length increases. Effectively, the conduction resistance increases. The boundary layer is interrupted at the peaks but is thicker in the troughs.

Disrupting the boundary layer along the wall of the fin with bumps, like the ones created using a sinewave, creates an overall decrease in the heat transfer coefficient. The bumps add a significant amount of area without actually increasing the heat transfer by a significant amount because of the corresponding reduction in the heat transfer coefficient associated with the stagnant air pockets. Figure 26 shows the ratio of the heat transfer coefficient of the wavy fin compared to the heat transfer coefficient of a smooth fin with the same average diameter as a function of the amplitude to diameter ratio.

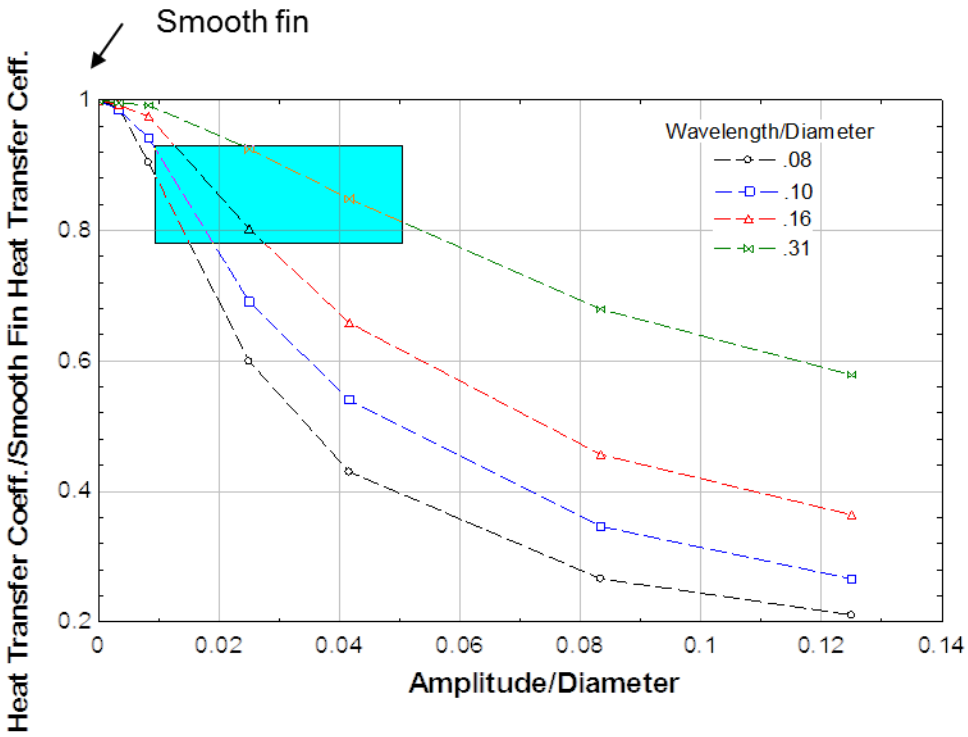

Figure 26: Opposed waviness heat transfer coefficient, with printed feature size highlighted blue

As the amplitude increases, the heat transfer coefficient decreases for all wavelength to diameter ratios. As the wavelength decreases, the heat transfer coefficient decreases as well. The wavelength to diameter ratio describes the number of “bumps” on the fin, the more bumps on a fin, the shorter the wavelength. The decrease in heat transfer coefficient with decreasing wavelength corresponds to an overall increase in surface area. In general, as more and larger bumps are added, the heat transfer coefficient decreases because of the way the flow gets caught in the troughs of the sinewaves. The range of surface area ratios explored in the study was from 0 up to 5 times the area of the smooth fin counterpart. For the fin with the largest area ratio, if the heat transfer coefficient of the wavy fin were to remain the same as the heat transfer coefficient of the smooth fin (corresponding to a ratio

of 1 on the y-axis of Figure 26), the heat transfer from the fin would need to be over 5 times that of the smooth fin heat transfer. At this most extreme geometry, the heat transfer coefficient ratio was about 0.2. The highlighted region of the figure represents the geometric region of the bumps found on the printed fins. There is little change in performance between a completely smooth fin and a fin with bumps similar in size to those found on the printed fins. The conductance of the fin is the product of the heat transfer coefficient and the surface area. The ratio of the conductance of the wavy fin to that of a smooth is shown as a function of the ratio of amplitude to diameter in Figure 27.

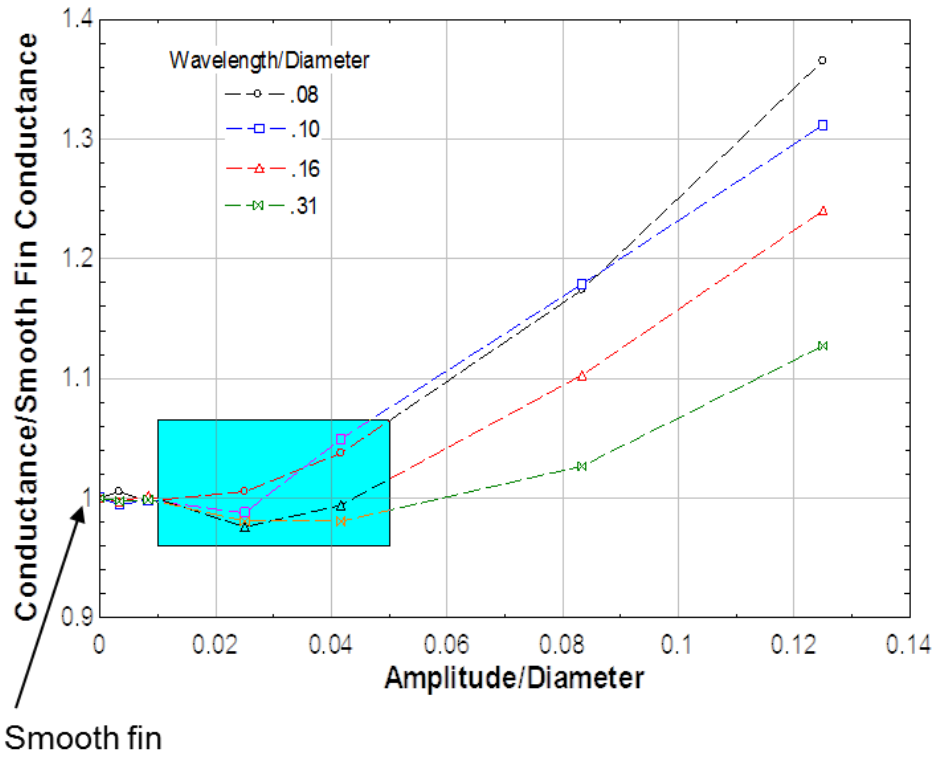

Figure 27: Opposed waviness conductance, with printed feature size highlighted in blue

The conductance of the fin increases with an increasing amplitude and a decreasing wavelength, corresponding to an increase in fin surface area. In the geometric region where the bumps on the printed fins are located, there is almost no noticeable change in conductance. At the most extreme geometric ratios, the conductance of the wavy fin is less than 1.4 times that of the smooth fin. While there is a slight increase in conductance with an increase in area, the area increases much more than the conductance, which is a symptom of reduction in the heat transfer coefficient.

The pressure drop ratio of the wavy fins compared to that of the smooth fin is shown in Figure 28 to analyze the hydraulic performance.

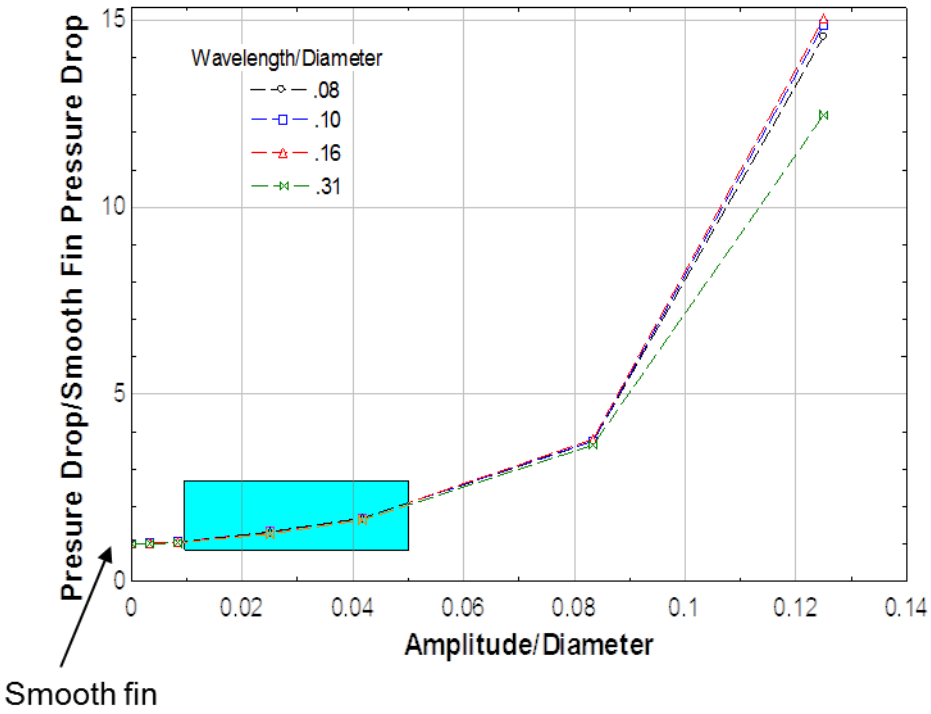

Figure 28: Opposed waviness pressure drop, with printed feature size highlighted in blue

The pressure drop increases with increasing amplitude and decreasing wavelength, corresponding to an increase in surface area. At the most extreme geometric ratios, the pressure drop of the wavy fin is 15 times that of the smooth fin. The pressure drop increases so significantly, because the fluid domain became very small at the geometric extremes. As there are more bumps and they get larger, there is more air caught in the troughs on the sinewave which translates to an even higher pressure drop. The change in pressure drop in the geometric region where printing takes place is insignificant. However, the small increase in conductance displayed by the wavy fin does not compare to the extreme increase in pressure drop at extreme geometric ratios. Across all velocities and Reynolds numbers, the thermal and hydraulic performance of the wavy fins was the same.

5.1.2. Opposed waviness thermal performance along circumference

To better understand the phenomenon of the reduction in heat transfer coefficient that occurs with increasing amplitude, the heat transfer coefficient along the circumference was computed based on the simulation results. In Fluent post-processing, the heat flux along the edge was exported and used to calculate a local heat transfer coefficient. At an angle of 0 degrees, the airflow first contacts the fin (airflow is from the bottom to the top of the page), as seen in Figure 29.

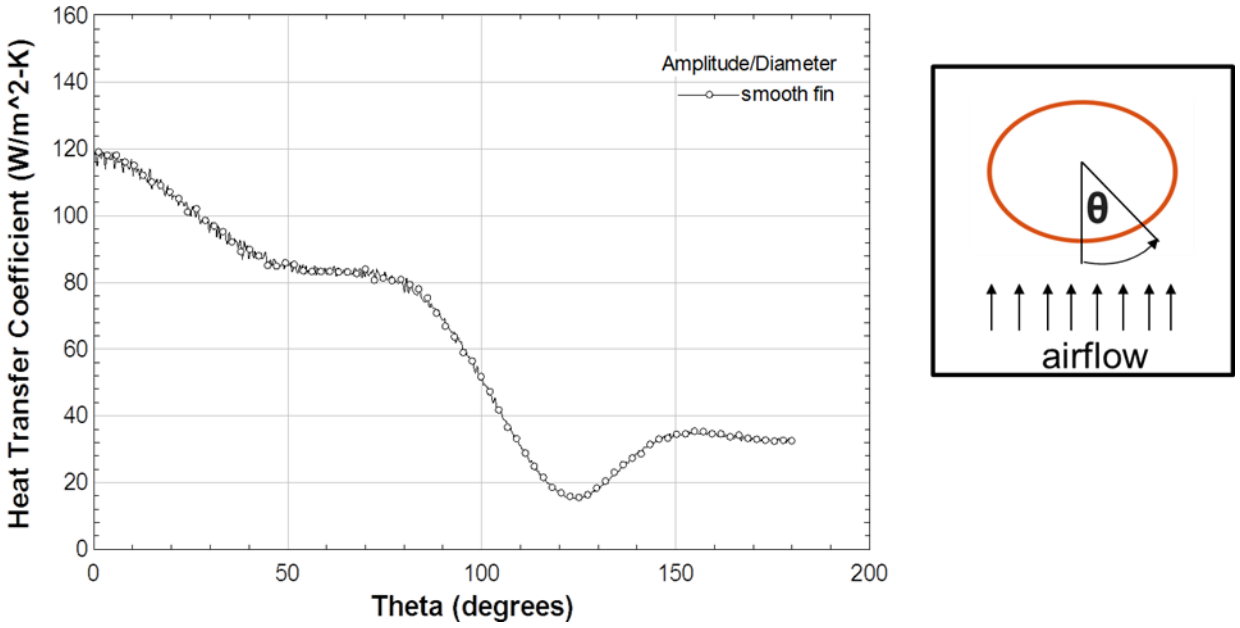

Figure 29: Circumferential heat transfer coefficient of smooth fin

The heat transfer coefficient of a smooth fin is initially largest at an angle of 0, where the flow first strikes the fin. An angle of 180 degrees marks the location opposite 0 degrees and is the point nearest to the pressure outlet. With increasing angle, the heat transfer coefficient decreases because the laminar boundary layer is developing. There is a larger decrease after 100 degrees where separation occurs and then the heat transfer coefficient increases due to mixing. The lowest heat transfer coefficient occurs at an angle of about 125 degrees, where the airflow almost bypasses the fin because it is accelerated to the pressure outlet. The heat transfer coefficient increases slightly until the pressure outlet due to some backflow and swirling flow near the outlet.

The wavelength was kept constant in order to understand the effect, solely, that the amplitude had on the heat transfer coefficient. Figure 30 shows the heat transfer coefficient

at a small amplitude to diameter ratio. The peaks in Figure 30 clearly identify the location of the peaks on the sinewave that is circumscribed on the fin. Again, it can be seen that in the troughs, the convective heat transfer coefficient decreases because the surface area for convection decreases. In comparison to the smooth fin, there is a larger heat transfer coefficient at the peaks of the wavy fin.

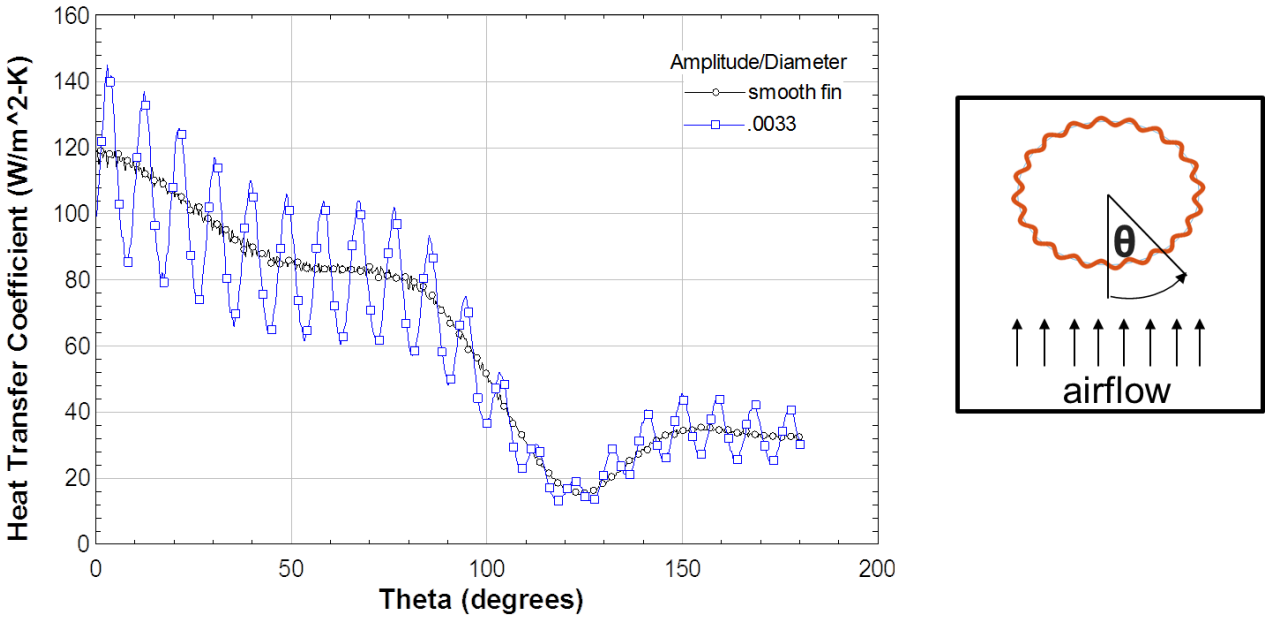

Figure 30: Circumferential heat transfer coefficient of aligned waviness fin at lower amplitude

Figure 31 shows the heat transfer coefficient at an even higher amplitude and compares it to the lower amplitude and smooth fin. The same trend of an increased heat transfer coefficient at the peak and a decreased heat transfer coefficient at the trough can be seen. It is also more apparent that the increase in heat transfer coefficient at the peak is not as large as the decrease in heat transfer coefficient in the trough. On average, the heat transfer coefficient decreases with an increase in amplitude because the heat transfer coefficient in the trough region decreases significantly.

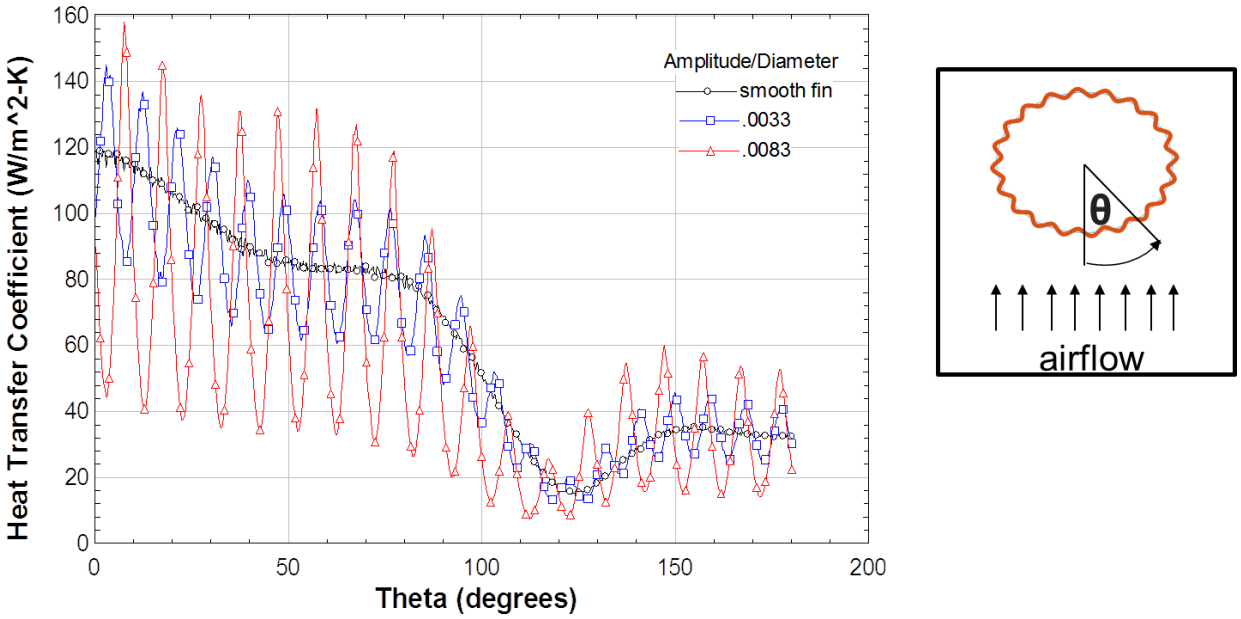

Figure 31: Circumferential heat transfer coefficient of aligned waviness fin at higher amplitude

The difference between the heat transfer coefficient of the lower amplitude and higher amplitude fins at the peaks is much smaller than the difference between the heat transfer coefficient of the lower amplitude and higher amplitude fins at the troughs. The region near an angle of 125 degrees does not see an increase in heat transfer coefficient at the peak, but it does see a slight decrease in the troughs, also contributing to the overall decrease in average heat transfer coefficient with an increase in amplitude. The backflow at this location coupled with the introduction of the peaks and troughs makes it a location of minimal heat transfer.

5.2. Aligned Waviness Results

5.2.1. Aligned waviness performance compared to smooth fin

The temperature and velocity distribution for the aligned waviness simulations are similar to the results seen for the smooth fin, presented in the last section. The main effect of the waviness can mainly be seen in the troughs of the sinewaves, which create slower moving

air. The temperature plots for an aligned waviness fin are shown in Figure 32.The range of amplitude to diameter ratio for the aligned waviness simulations was narrowed to explore bumps that might occur from choice of print direction instead of bumps that would be significant in size compared to the total feature size.

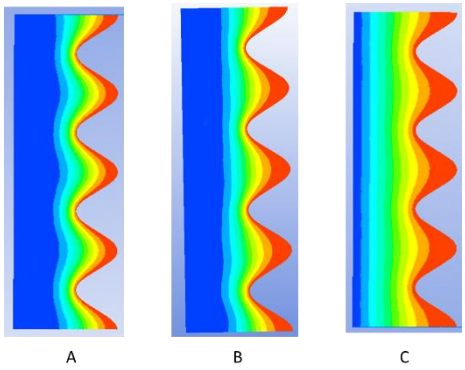

Figure 32: Aligned waviness temperature contours at (A) inlet (B) midplane of fin and (C) outlet

In Figure 32, the temperature contour plot shows that there is initially a large temperature difference within the troughs at the inlet of the fluid domain. Because air is just entering, the temperature difference should be large. There is a smaller temperature difference within the trough at the outlet.

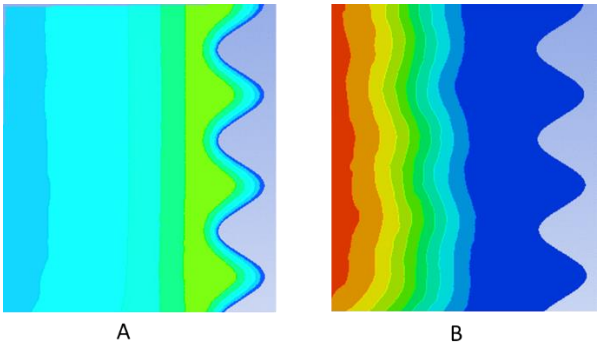

Figure 33: Aligned waviness velocity contours for (A) a plane near inlet and (B) a plane near the outlet

In Figure 33, the velocity vectors at the inlet are very slow, corresponding to the blue color, upon initial contact with the fin. The faster moving air can be seen near the outlet of the fin which corresponds to the red. To better understand the temperature distribution at the various points along the height of the fin, Figure 34.A shows the temperatures at the trough and Figure 34.B shows the temperatures at the peak. The airflow is from left to right.

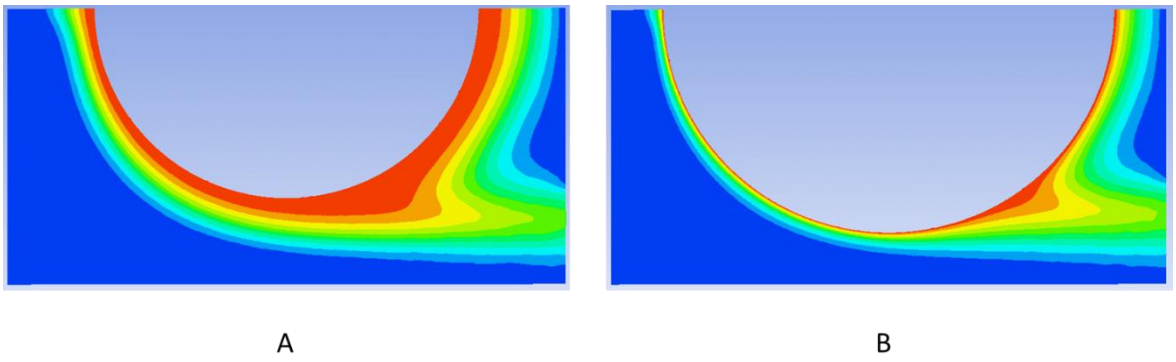

Figure 34: Aligned waviness temperature contour at (A) the trough and (B) the peak

Larger bands of warmer air can be seen surrounding the fin at the trough. There is a larger temperature gradient at the peak, which corresponds to a higher heat flux. The velocity contour at the trough and the peak is shown in Figure 35.A and Figure 38.B, respectively. The air at the trough is much more slow-moving than the air at the peak. The air at the peak also has larger velocities along the circumference of the fin.

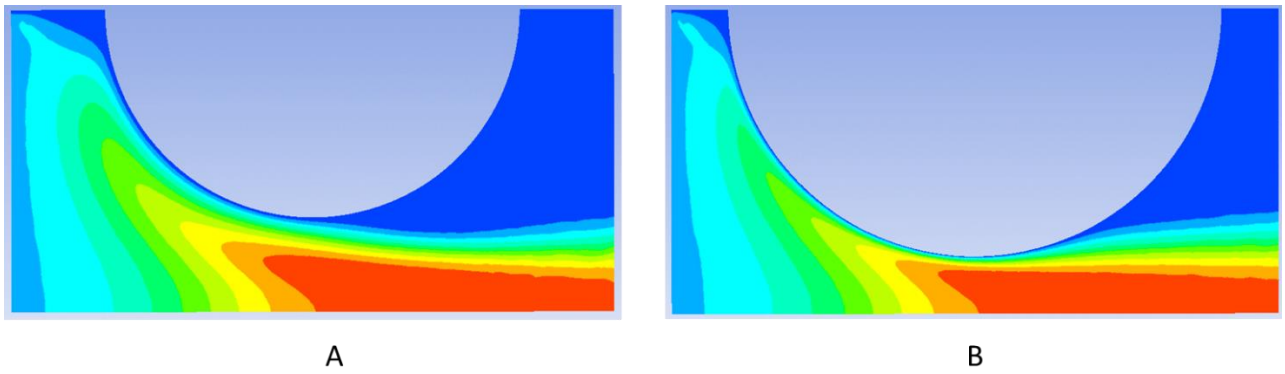

Figure 35: Aligned waviness velocity contours at (A) the trough and (B) the peak

The warmer, slow-moving air in the trough does not perform as well thermally as the air at the peak. In the next section, the heat transfer coefficient as a function of theta at various locations along the height of the fin will be further explored.

The average heat transfer coefficient of the fins decreased with an increasing amplitude and decreasing wavelength. The fin at the smallest wavelength saw a very insignificant change in the heat transfer coefficient. As the amplitude increased and the wavelength decreased, the heat transfer coefficient decreased. As the amplitude increases, the air travels at a slower velocity through the trough.

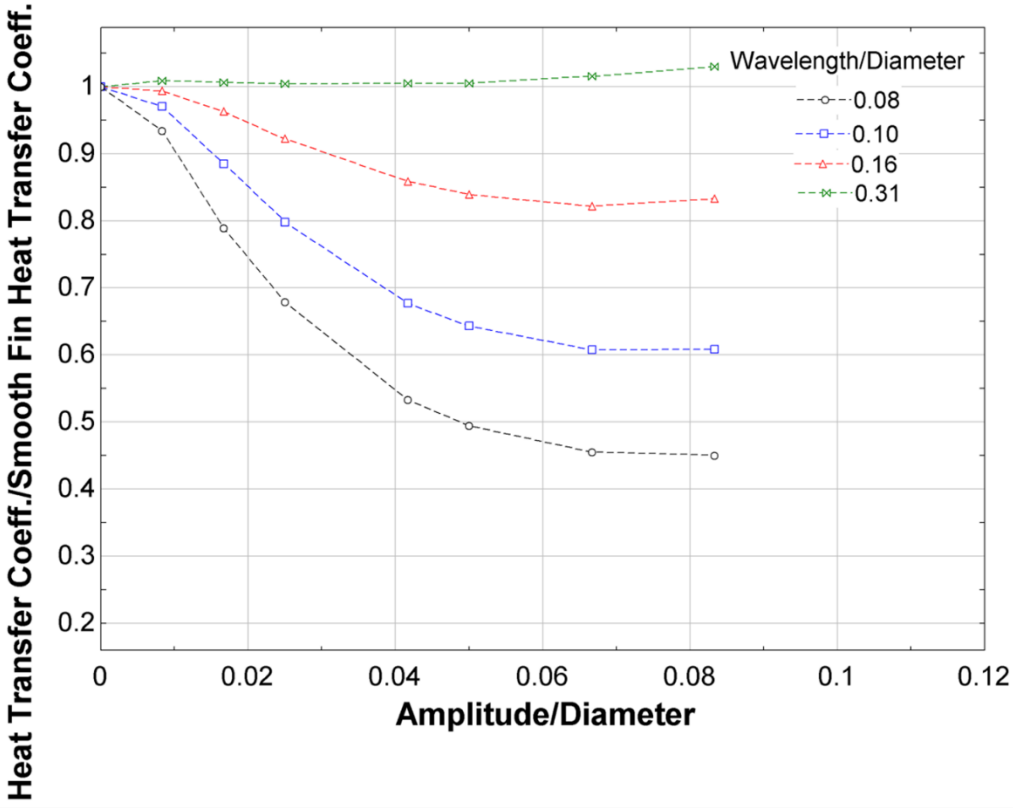

Figure 36: Aligned waviness heat transfer coefficient

The conductance of the fins is shown in Figure 37.The conductance at the longest wavelength performs the worst. There is little difference in the conductance for the other three wavelengths. Because the conductance of these fins is almost the same and the areas differ significantly, the heat transfer coefficients must decrease according to decreasing wavelength, as seen in the previous figure.

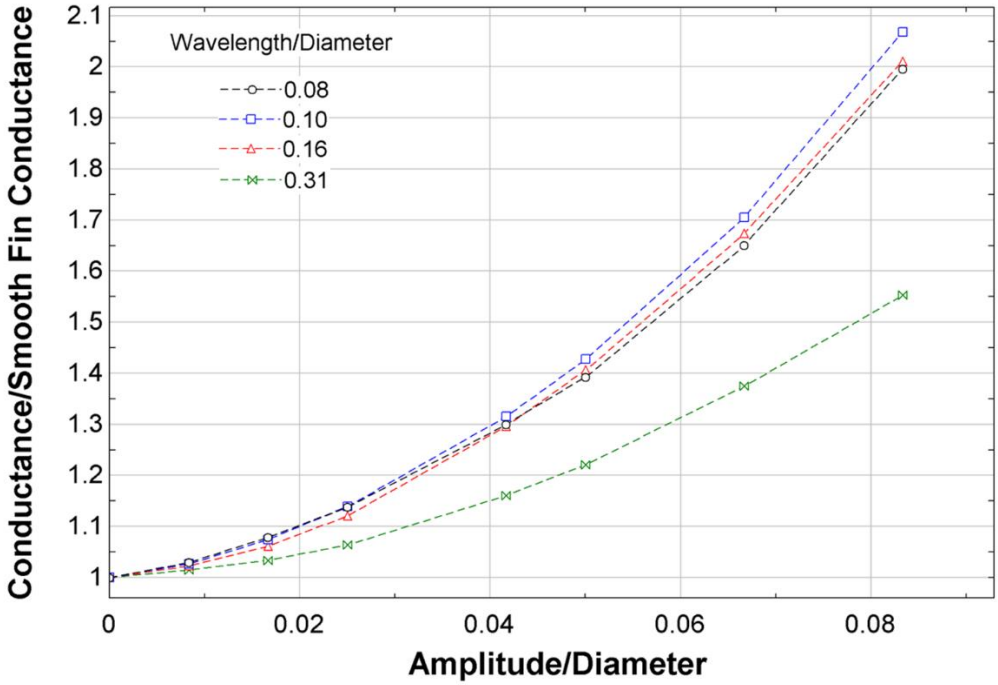

Figure 37: Aligned waviness conductance

The pressure drop increases only slightly for the aligned waviness fins. The increase in pressure drop is detailed in Figure 38. The slowest airflow at higher amplitudes is through the trough. Air accelerates on either side of the peak because there is no fin there to slow it down.

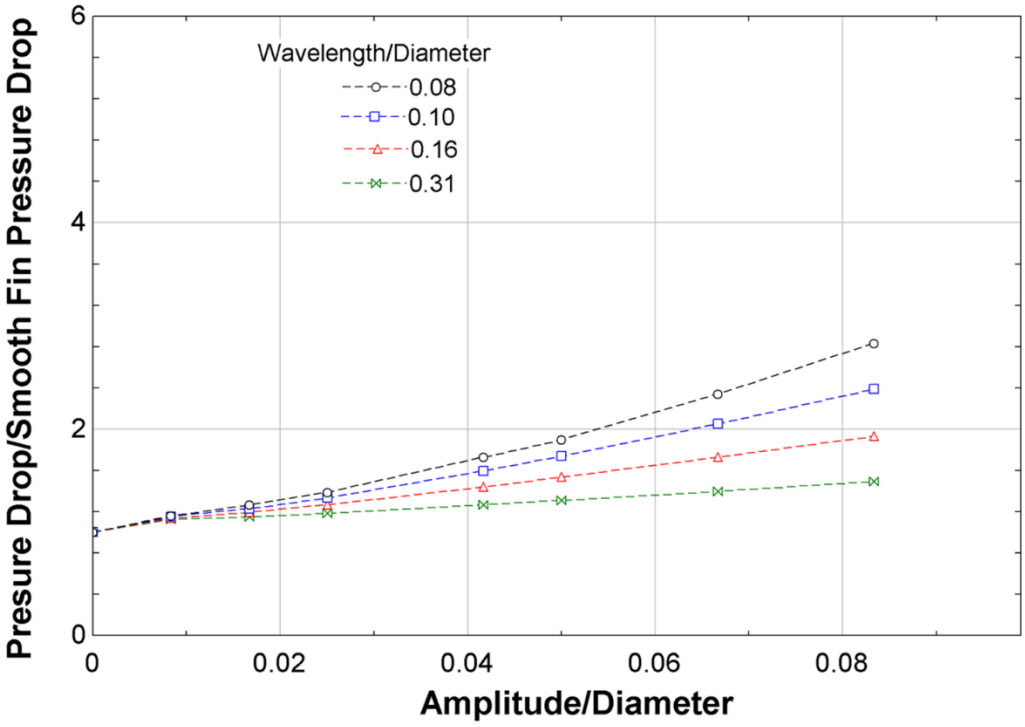

Figure 38: Aligned waviness pressure drop

5.2.2. Aligned waviness performance along circumference

The heat transfer coefficient along the circumference of the fin at various locations along the fin height is detailed in Figure 39. The amplitude used in the simulation corresponds to the lowest amplitude to diameter ratio in the study. The heat transfer coefficient at the average diameter is the same as the heat transfer coefficient for a smooth fin for most angles. The aligned waviness fin creates a smaller heat transfer coefficient initially at the inlet for all locations along the height of the fin. This may be due to the restricted fluid domain.

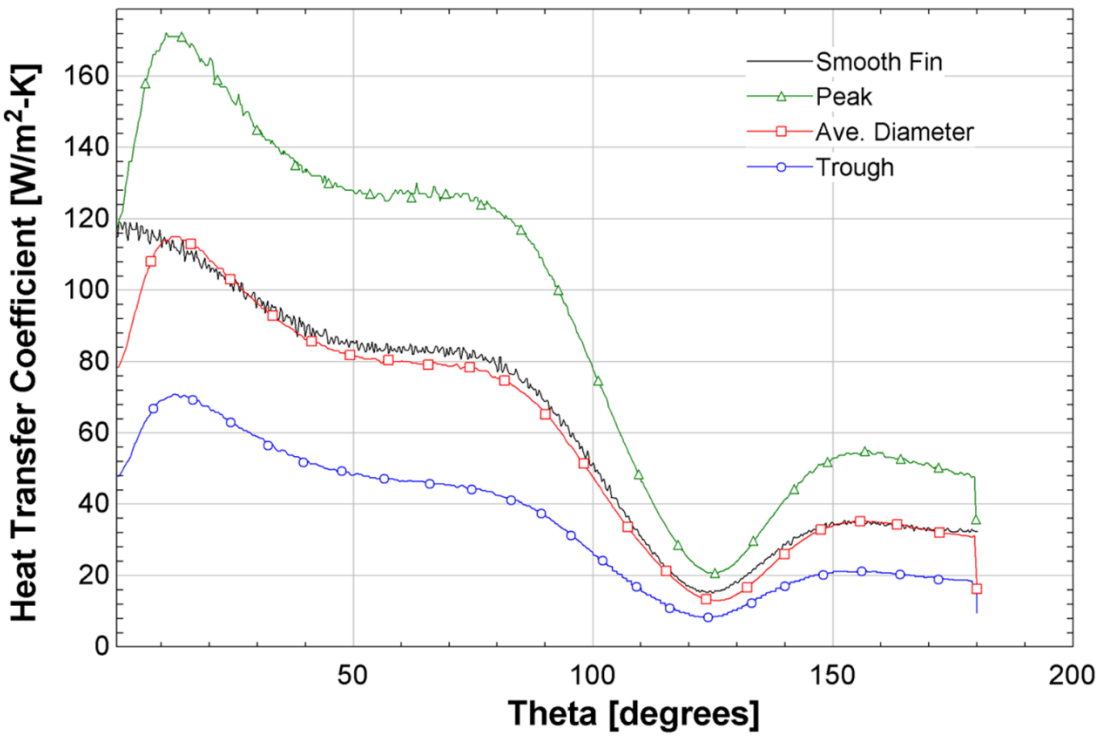

Figure 39: Aligned waviness heat transfer coefficient along circumference at lower amplitude

The difference in the highest heat transfer coefficient at the peak and the heat transfer coefficient at the average diameter is larger than the difference in the highest heat transfer coefficient at the trough and the heat transfer coefficient at the average diameter. At other locations, that is not the case because, on average, the heat transfer coefficient of the smooth fin is larger than the heat transfer coefficient of the aligned waviness fin. Near 100 degrees, the difference between the heat transfer coefficient at the trough and the heat transfer coefficient at the average diameter is larger than the difference between the heat transfer coefficient at the peak and the heat transfer coefficient at the average diameter.

The heat transfer coefficient along the circumference for a larger amplitude is show in Figure 40.

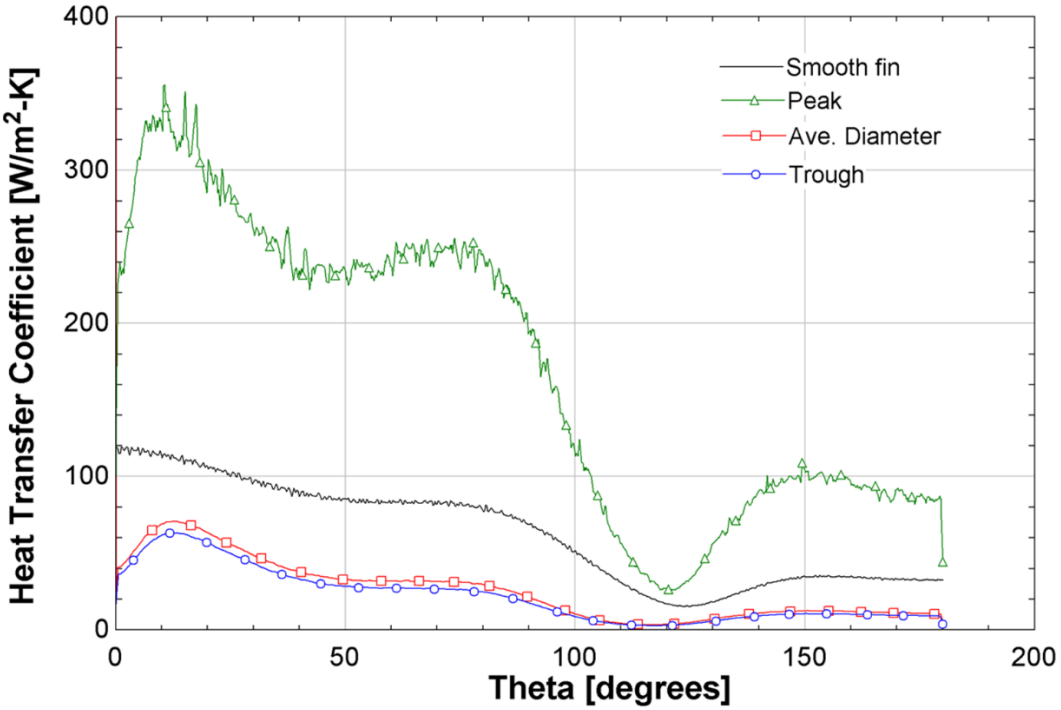

Figure 40: Aligned waviness heat transfer coefficient along circumference for higher amplitude

As the amplitude increases, the heat transfer coefficient at the peak increases substantially. The increase in heat transfer coefficient at the peak comes at the cost of less heat transfer near the trough and the average diameter. Much of the heat transfer is taking place near the peaks, leaving the other areas of the fin ineffective. The heat transfer in a larger amplitude fin is concentrated on the peak with a drastic change over the period of the sinewave.

5.3. Opposed vs. Aligned Waviness Comparison and Correction Factor

The aligned waviness fins performed, both thermally and hydraulically, better than the opposed waviness fins. The heat transfer coefficients are compared in Figure 41. In this figure, the solid red lines represent the opposed waviness fins and the dotted blue line represents the aligned waviness fins. While the heat transfer coefficients decrease in both cases, the heat transfer coefficients for the aligned waviness fins don't decrease as much as the heat transfer coefficient for the opposed waviness fins.

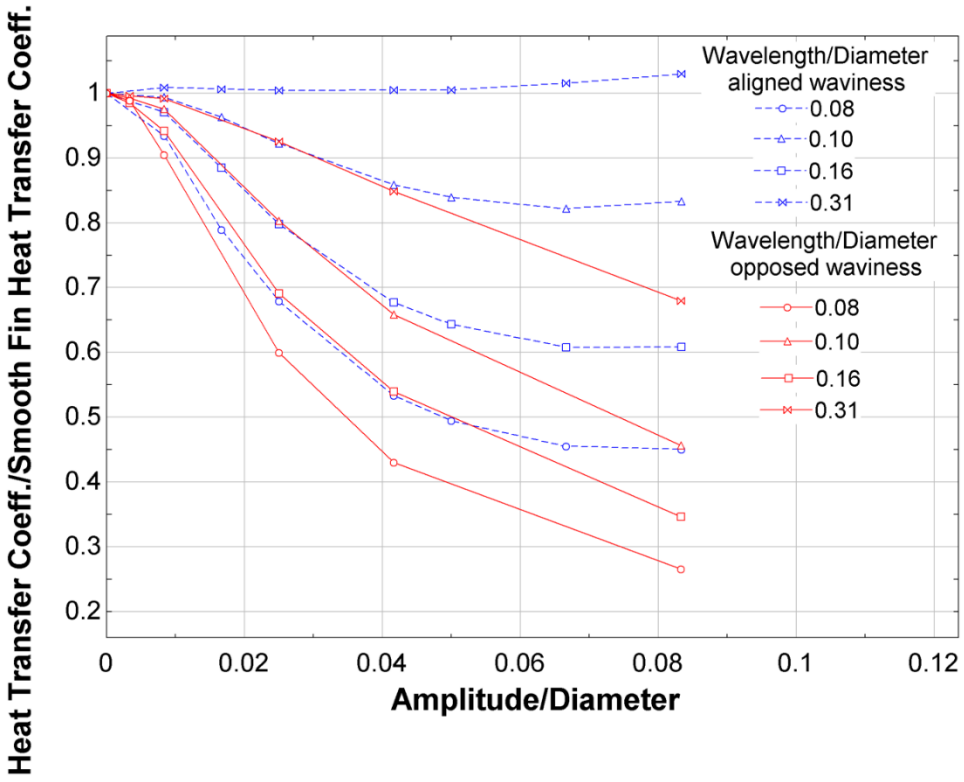

Figure 41: Heat transfer coefficient for aligned and opposed waviness fins

The aligned waviness fins also have better conductance than the opposed waviness fins. The conductance for the aligned waviness fins is shown in Figure 42. Even at the largest

amplitudes of the opposed waviness fins, the conductance never reached a ratio of 2. For the three smallest wavelengths in the aligned waviness simulations, the conductance did reach a ratio near 2 due to the fact that the peaks in the aligned waviness fins created more heat transfer than the peaks in the opposed waviness fins.

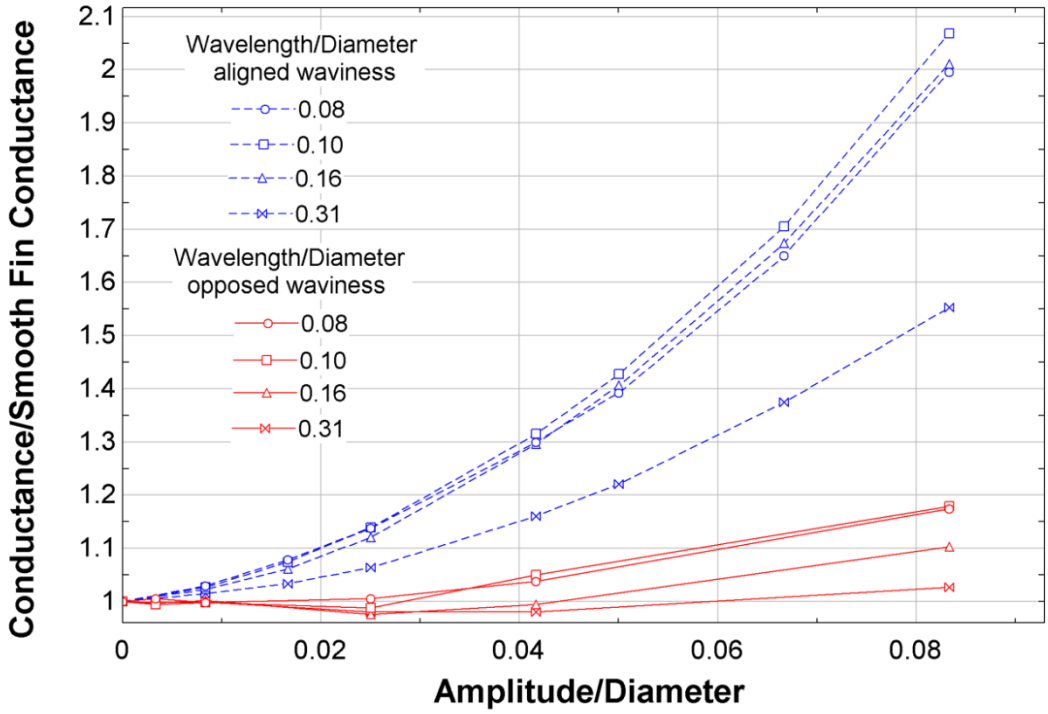

Figure 42:Conductance for aligned and opposed waviness fins

The pressure drops of both the aligned and opposed simulations are compared in Figure 43. While there is a smaller pressure drop in the aligned fins, the pressure in the opposed fins is only slightly higher. There is also a larger difference in pressure drop as the wavelength is varied in the aligned waviness fins than in the opposed waviness fins. For the aligned fins,

the number of bumps is more important to the velocity and flow of the fluid. As more bumps are introduced, there are more obstructions in the fluid's path.

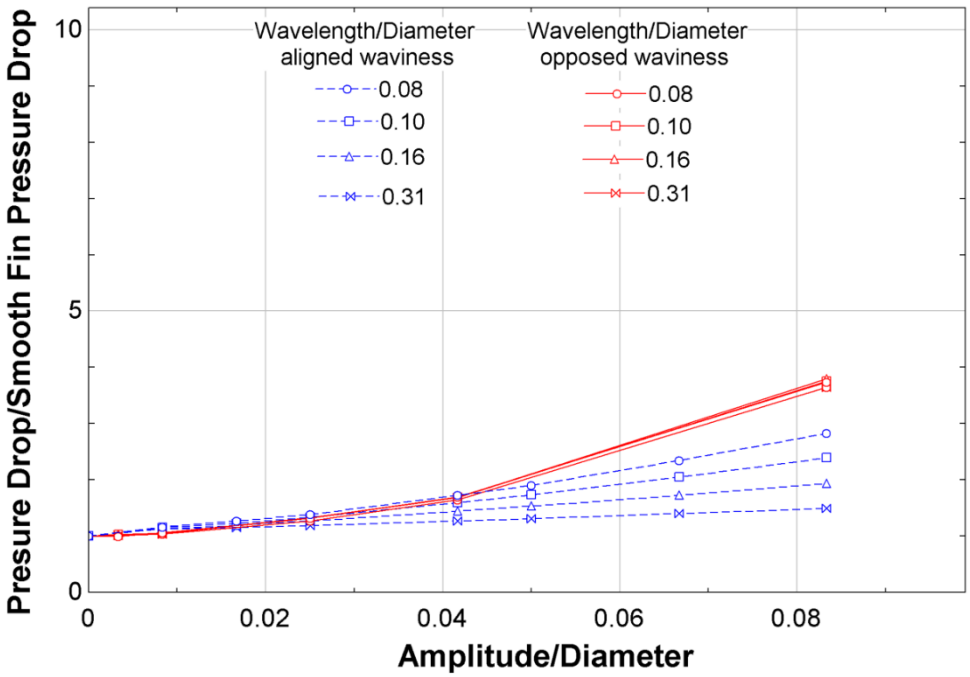

Figure 43:Pressure drop for aligned and opposed waviness

In both cases, the performance in the trough decreases the overall performance of the fin. In the opposed waviness simulations, the performance in the trough decreases the overall heat transfer significantly in comparison to the performance in the trough of the aligned waviness fins. From these results, correction factors can be created in order to understand how a fin's performance might change based on the quality or "bumpiness" of the print. Third order polynomials were used to create the following correction factors at this smaller range of amplitude to diameter ratios. The correction equation for the heat transfer coefficient for an opposed waviness fin is as follows:

$$\overline{h_{wavy}} = \left[0.63404 + 8.21355\left(\frac{W}{D}\right) - 48.6992\left(\frac{W}{D}\right)^2 + 85.3504\left(\frac{W}{D}\right)^3 - 26.59767\left(\frac{A}{D}\right) + 190.45782\left(\frac{A}{D}\right)^2 - 285.79858\left(\frac{A}{D}\right)^3 + 113.01385\left(\frac{W}{D}\right)\left(\frac{A}{D}\right) - 823.28328\left(\frac{W}{D}\right)\left(\frac{A}{D}\right)^2 - 162.68921\left(\frac{W}{D}\right)^2\left(\frac{A}{D}\right) + 1327.49203\left(\frac{W}{D}\right)^2\left(\frac{A}{D}\right)^2\right]\overline{h_{smooth}} \quad (8)$$

These corrections can be used to predict performance of future printed fins at various geometric ratios within the range of wavelength to diameter and amplitude to diameter ratios that were simulated. The equations for the remaining heat transfer coefficient corrections can be found in Appendix B. The heat transfer coefficient correction fits the opposed waviness data as shown in Figure 44.

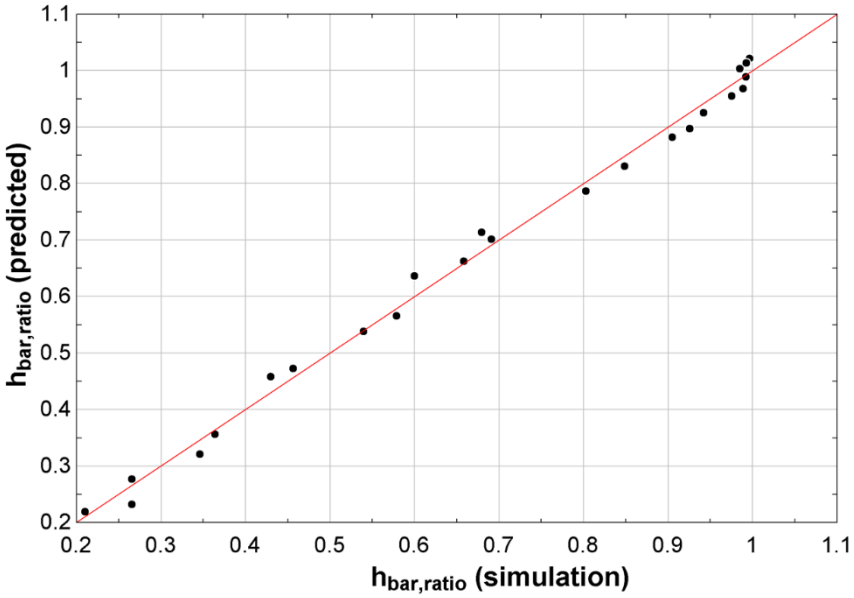

Figure 44: Opposed waviness heat transfer coefficient predicted compared to simulation data

The pressure drop correction equations are referenced in Appendix B as well.

6. Conclusions

The opposed waviness fins were simulated in order to understand how the bumpiness present on the printed fins affects performance. In these simulations, the bumps that were similar in size to the bumps on the printed fins created almost no noticeable change in the thermal and hydraulic performance. The results of these simulations also revealed that there exists an unfavorable geometric region for the size of the bumps. In this region, a large pressure drop is created with a small increase in heat transfer. Printed imperfections that create a ratio of the extension of the imperfection beyond the actual feature to the

entire feature's size above 0.05 start creating undesirable performance. The best-fit curve created can help predict performance of printed features.

The aligned waviness fins were simulated in order to see if there was a direction in which the waviness could be advantageous. The aligned waviness fins proved to perform better than the opposed waviness fins. At the same geometric ratios, the aligned waviness created a higher heat transfer coefficient and lower pressure drop than the opposed waviness. The choice in print direction is dependent on many different factors. If the print direction could be chosen such that aligned waviness resulted, the heat transfer would improve with only a small increase in pressure drop.

7. References

[1] DOE, "ARPA-E Program Overview," 2016.

[2] V. Tidwell and G. Klise, "Exploring the Water-Thermoelectric Power Nexus," *Journal of Water Resources Planning and Management*, vol. 135, 2012.

[3] C. Leeds, "Simulation of Tapered Fins and Cylinders in Crossflow," M>S> thesis, Dept. Mech. Eng., Univ. of Wisc., Madison, WI, 2016

[4] J. Boxleitner, "Additive Design and Manufacturing of a Composite Polymer Heat Exchanger," in *17th International Refrigeration and Air Conditioning Conference* West Lafayette, IN, 2018.

[5] F. Incropera, D. DeWitt, T. Bergman, A. Levine, *Fundamentals of Heat and Mass Transfer,* 6th ed. Hoboken, NJ: John Wiley & Sons, 2007.

8. Appendix A

```
clc
clear
%Wavy geometry creator
%Creates sinewave around a circle
```

```
%Can specify the amplitude and frequency of the wave
%Uses parametric equations

t0=0;   %initial t
t1=2*pi;    %final t
N=1500;  %number of points
D_rad=(t1-t0)/(N-1);    %step size in radians
t=linspace(t0,t1,N);

%parameters to vary
R=3;
A=0.25;
F=20;

%parametric equations for x and y

for i=1:numel(t-1)
   x(i)=(R+A*sin(F*t(i)))*cos(t(i));
   y(i)=(R+A*sin(F*t(i)))*sin(t(i)) ;
   z(i)=zeros(numel(N-1),1);
end

%Additional text file components
Group=[ones(numel(t-1),1)];
Point=[1:numel(t-1)]';
Point(600)=0;

%  for i=1:numel(t)
%      x(i)=cos(t(i));
%      y(i)=sin(t(i));
%      z(i)=zeros(numel(N),1);
%  end
theta=0:.01:2*pi;
rx=3*cos(theta);
ry=3*sin(theta);


plot(rx,ry,'-')
hold on
plot(x,y,'*')
xlim([-4 4])
ylim([-4 4])
hold off

f=fopen('ParabolicCoordinates.txt','w');
fprintf(f,'%s\t%s\t%s\t%s\t%s\r\n', '#Group', 'Point','X','Y','Z');
```

```
for j=1:numel(t)-1
   fprintf(f,'%d\t\r%d\t\r%.3f\t\r%.3f\t\r%d\t\r\n', Group(j), Point(j), x(j), y(j), z(j));
end
fprintf(f,'%d\t\r%d\t\r', Group(N), Point(N));
fclose(f)

Group1=1:1:numel(x);
Point1=1:1:numel(x);
f=fopen('ParabolicCoordinates2.txt','w');
fprintf(f,'%s\t%s\t%s\t%s\t%s\r\n', '#Group', 'Point','X','Y','Z');
for j=1:numel(t)-1
   fprintf(f,'%d\t\r%d\t\r%.3f\t\r%.3f\t\r%d\t\r\n', Group1(j), Point1(j), x(j), y(j), z(j));
end
fprintf(f,'%d\t\r%d\t\r', Group(N), Point(N));
fclose(f)
```

9. Appendix B

Aligned waviness heat transfer coefficient correction:

$$\overline{h_{wavy}} = \left[0.40785 + 14.34448\left(\frac{W}{D}\right) - 90.29046\left(\frac{W}{D}\right)^2 + 162.76215\left(\frac{W}{D}\right)^3 - 35.33591\left(\frac{A}{D}\right) + 279.12762\left(\frac{A}{D}\right)^2 - 247.68132\left(\frac{A}{D}\right)^3 + 244.12416\left(\frac{W}{D}\right)\left(\frac{A}{D}\right) - 1788.22878\left(\frac{W}{D}\right)\left(\frac{A}{D}\right)^2 - 440.78034\left(\frac{W}{D}\right)^2\left(\frac{A}{D}\right) + 3331.97392\left(\frac{W}{D}\right)^2\left(\frac{A}{D}\right)^2\right]\overline{h_{smooth}}$$

Opposed waviness pressure drop correction:

$$\Delta p_{wavy} = \left[2.07594 + 21.25517\left(\frac{W}{D}\right) + 133.01692\left(\frac{W}{D}\right)^2 - 240.13228\left(\frac{W}{D}\right)^3 + 10.91098\left(\frac{A}{D}\right) + 340.90091\left(\frac{A}{D}\right)^2 - 496.72351\left(\frac{A}{D}\right)^3 - 39.66675\left(\frac{W}{D}\right)\left(\frac{A}{D}\right) - 2282.73664\left(\frac{W}{D}\right)\left(\frac{A}{D}\right)^2 + 22.58807\left(\frac{W}{D}\right)^2\left(\frac{A}{D}\right) + 4713.38573\left(\frac{W}{D}\right)^2\left(\frac{A}{D}\right)^2\right]\Delta p_{smooth}$$

Aligned waviness pressure drop correction:

$$\Delta p_{wavy} = \left[-2.46418 + 73.26462\left(\frac{W}{D}\right) - 485.76489 + 915.93906\left(\frac{W}{D}\right)^3 - 1.62236\left(\frac{A}{D}\right) - 754.52766\left(\frac{A}{D}\right)^2 + 15491.7921\left(\frac{A}{D}\right)^3 + 745.16024\left(\frac{W}{D}\right)\left(\frac{A}{D}\right) - 10047.2816\left(\frac{W}{D}\right)\left(\frac{A}{D}\right)^2 - 1892.33484\left(\frac{W}{D}\right)^2\left(\frac{A}{D}\right) + 25456.0040\left(\frac{W}{D}\right)^2\left(\frac{A}{D}\right)^2\right]\Delta p_{smooth}$$